Atmos. Chem. Phys., 13, 1547–1567, 2013
www.atmos-chem-phys.net/13/1547/2013/
doi:10.5194/acp-13-1547-2013

Atmospheric Chemistry and Physics Open Access

Tropospheric NO_2 vertical column densities over Beijing: results of the first three years of ground-based MAX-DOAS measurements (2008–2011) and satellite validation

J. Z. Ma[1], S. Beirle[2], J. L. Jin[1,*], R. Shaiganfar[2], P. Yan[1,*], and T. Wagner[2]

[1]Chinese Academy of Meteorological Sciences, Beijing, China
[2]Max Planck Institute for Chemistry, Mainz, Germany
[*]now at: CMA Meteorological Observation Centre, Beijing, China

Correspondence to: J. Z. Ma (mjz@cams.cma.gov.cn)

Received: 12 July 2012 – Published in Atmos. Chem. Phys. Discuss.: 11 October 2012
Revised: 21 December 2012 – Accepted: 7 January 2013 – Published: 7 February 2013

Abstract. Ground-based measurements of scattered sunlight by the Multi Axis Differential Optical Absorption Spectroscopy (MAX-DOAS) have been carried out at an urban site (39.95° N, 116.32° E) in Beijing megacity since 6 August 2008. In this study, we retrieved the tropospheric NO_2 vertical column densities (VCDs) over Beijing from these MAX-DOAS observations from August 2008 to September 2011. Over this period, the daytime (08:00–17:00 Beijing Time (BJT, which equals UTC + 8)) mean tropospheric NO_2 VCDs varied from 0.5 to 13.3 with an average of 3.6 during summertime, and from 0.2 to 16.8 with an average of 5.8 during wintertime, all in units of 10^{16} molecules cm^{-2}. The average diurnal variation patterns of tropospheric NO_2 over Beijing appeared to be rather different from one season to another, indicating differences in the emission strength and atmospheric lifetime. In contrast to previous studies, we find a small weekly cycle of the tropospheric NO_2 VCD over Beijing. The NO_2 VCD in the late afternoon was the largest on Saturday and the lowest on Sunday, and in the morning it reached a clear maximum on Wednesday. We also find a post-Olympic Games effect, with 39–54 % decrease in the tropospheric NO_2 VCD over Beijing estimated for August of 2008, compared to the following years. The tropospheric NO_2 VCDs derived by our ground MAX-DOAS measurements show a good correlation with SCIAMACHY and OMI satellite data. However, compared with the MAX-DOAS measurements, the satellite observations underestimate the tropospheric NO_2 VCDs over Beijing systematically, by 43 % for SCIAMACHY and 26–38 % for OMI (DOMINO v2.0 and DOMINO v1.02). Based on radiative transfer simulations, we show that the aerosol shielding effect can explain this underestimation, while the gradient smoothing effect caused by the coarse spatial resolution of the satellite observations could play an additional role.

1 Introduction

Nitrogen dioxide (NO_2) is an important trace gas in the troposphere. It participates in the control of the strong oxidant, O_3, and the strongest atmospheric oxidizing agent, OH, acts as gaseous precursor of aerosols and acid rain, and contributes locally to radiative forcing of climate (Seinfeld and Pandis, 1998; Solomon et al., 1999; Lelieveld and Dentener, 2000; Lelieveld et al., 2002). In addition, NO_2 is known to cause respiratory problems for humans in the urban atmosphere, and has been listed as one of primary pollutants with national ambient air quality standards in many countries, including China (SEPA, 1996; EPA, 2000). Increasing traffic, power generation and industrial activities, especially in megacities (> 10 million population), provide immense sources of nitrogen oxides ($NO_x \equiv NO + NO_2$) and other pollutants, degrading air quality and adversely affecting human health (Molina and Molina, 2004).

With the launch of a series of satellites ERS-2, ENVISAT, AURA and METOP since 1995, information on the global distribution of total and tropospheric NO_2 columns have become available from the on-boarded instruments, named

Global Ozone Monitoring Experiment (GOME), SCanning Imaging Absorption spectroMeter for Atmospheric CHartographY (SCIAMACHY), Ozone Monitoring Instrument (OMI) and GOME-2, respectively (e.g. Burrows et al., 1999b; Bovensmann et al., 1999; Levelt et al., 2006; Valks et al., 2011). The retrievals of the NO_2 columns from these ultraviolet-visible (UV-VIS) measurements are based on the technique of differential optical absorption spectroscopy (DOAS) (Platt, 1994; Platt and Stutz, 2008; Wagner et al., 2008). The tropospheric NO_2 vertical column densities (VCDs) derived from satellite measurements have been used to study the NO_2 fields on both global and regional scales, including its emission variations and trends in severely polluted "hotspots", such as eastern China (e.g. Beirle et al., 2003; Richter et al., 2005; Ma et al., 2006; van der A et al., 2006, 2008; Zhao et al., 2006; Wang et al., 2007b; Zhang et al., 2007; Shi et al., 2008; Hayn et al., 2009; Lin et al., 2010; Lin and McElroy, 2011; Lin, 2012). Satellite measurements of tropospheric NO_2 were also applied to evaluate the weekly cycle and seasonal variation of urban air quality in Beijing (Beirle et al., 2003; Jiang et al., 2006) and the effects of emission control measures during the November 2006 Sino-African Summit (Wang et al., 2007a) and the August–September 2008 Olympic Games (Mijling et al., 2009; Witte et al., 2009; Yu et al., 2010). A range of about 40–60 % reductions of tropospheric NO_2 over Beijing during the 2008 Olympic Games was detected (Mijling et al., 2009; Witte et al., 2009; Yu et al., 2010). While the seasonal variation of tropospheric NO_2 is clearly obvious (Jiang et al., 2006), no weekend effect was found over Beijing (Beirle et al., 2003; Hayn et al., 2009).

Tropospheric NO_2 VCDs were retrieved from GOME with a precision of 35–60 % over regions with a large contribution of the troposphere to the total column (Boersma et al., 2004). There are still considerable biases in the satellite NO_2 products from SCIAMACHY, OMI and GOME-2, though improvements in the tropospheric NO_2 column retrieval algorithm have been made recently (e.g. Beirle et al., 2010; Boersma et al., 2011; Leitão et al., 2010; Richter et al., 2011; Valks et al., 2011). Tropospheric NO_2 over highly polluted areas accumulates predominantly (by more than 90 %) in the planetary boundary layer (PBL) (Ma et al., 2006). Considering the sensitivity of satellite observations to pollution located near the ground, as well as the uncertainties contained in satellite retrieval processes, ground-based measurements of tropospheric NO_2 columns and its vertical distributions are needed to validate the satellite observations.

Ground-based measurements of scattered light by the Multi Axis DOAS (MAX-DOAS) technique (Platt, 1994; Hönninger et al., 2004; Wagner et al., 2004; Wittrock et al., 2004), using a range of viewing angles from nearly horizontal through zenith, are especially sensitive to the tropospheric part of the NO_2 column, and can be used effectively to validate the satellite tropospheric NO_2 products. For example, MAX-DOAS instruments have been used to validate the OMI tropospheric NO_2 data over the urban (Kramer et al., 2008) and rural (Brinksma et al., 2008; Celarier et al., 2008; Hains et al., 2010) areas in Europe and India (Shaiganfar et al., 2011) as well as urban (Li et al., 2012) and mountain (Irie et al., 2008) areas in China. In addition, MAX-DOAS measurements provide important information about the vertical distributions and diurnal cycles of tropospheric NO_2 over selected interesting areas, which cannot be gained from satellite observations. Such information is important for the study of emission sources, chemical and transport processes, and for the quantitative comparison with model simulations. For instance, mobile MAX-DOAS measurements have been used to quantify NO_x emissions from the cities in Europe (Ibrahim et al., 2010; Wagner et al., 2010) and India (Shaiganfar et al., 2011).

Air quality in Beijing megacity has been of great concern in the atmospheric and environmental science community as well as public media (e.g. Stone, 2008; Parrish and Zhu, 2009). In order to investigate the photochemical pollution status as well as its formation mechanism and control policy, the concentrations of NO_2 near the ground, together with other chemical species and environmental parameters, were measured in Beijing during intensive field experiments over the past years, mostly using the chemiluminescence method (e.g. Tang et al., 2009; Lu et al., 2010; Wang et al., 2010b; Chou et al., 2011; Lin et al., 2011; Xu et al., 2011). Average NO_2 concentrations were estimated to be 30–40 ppbv for different seasons at the urban sites, with the hourly maximum reaching to 114 ppbv (Tang et al., 2009; Lin et al., 2011). Measurements of NO_2 concentrations in the PBL of Beijing, based on the long-path DOAS (LP-DOAS) technique, were carried out in a case study (Zhu et al., 2009, 2010). During the same experiment, a recently-developed MAX-DOAS instrument was also tested, measured tropospheric NO_2 VCDs were compared with those deduced from the LP-DOAS measurements and PBL heights, and the results showed a good correlation (Jin et al., 2010).

We have performed ground-based MAX-DOAS measurements in Beijing since 6 August 2008. For this study, the three years' DOAS spectra data obtained from August 2008 to September 2011 were analyzed with a focus on the tropospheric NO_2 column. In Sect. 2, we introduce our experiment and methods, including the observation site and instrument, spectral retrieval software and technique, and radiative transfer model and its application to our analysis. In Sect. 3, we present the results of the retrieved tropospheric NO_2 VCDs over Beijing, including the diurnal, weekly and seasonal variations, source emission and cloud effects, and comparisons with satellite data. Summary and conclusions are given in Sect. 4.

2 Experimental and methods

2.1 Site and instrument

Our measurement site (39.95° N, 116.32° E, 96 m a.s.l.) is located in the courtyard of China Meteorological Administration (CMA), Beijing. As described in previous studies (Sun et al., 2010; Lin et al., 2011), the CMA is situated in the northwest of the Beijing urban area, between the 2nd and 3rd Ring Roads, at about 3 km and 1.7 km distances from the 2nd and 3rd Ring Roads, respectively (Fig. 1). Our measurement platform was set up on the roof of a 10-story building. In situ measurements of gas pollutants were also carried out at this site during a different period (Lin et al., 2011).

The compact and relatively small (13 cm × 19 cm × 14 cm) Mini MAX-DOAS instrument from Hoffmann Messtechnik GmbH in Germany has been operated quasi-continuously in CMA since 6 August 2008. This instrument is designed for the spectral analysis of scattered sunlight and the application of the MAX-DOAS technique (Hönninger et al., 2004). The same type of instrument was used in previous studies, e.g. during the Dutch Aerosol and Nitrogen Dioxide Experiments for Validation of OMI and SCIAMACHY (DANDELIONS) (Brinksma et al., 2008) or the Cabauw Intercomparison campaign for Nitrogen Dioxide measuring Instruments (CINDI) (Piters et al., 2012). The instrument consists of a hermetically sealed metal box of approximately 3 L volume containing entrance optics, fiber coupled spectrograph and all electronics. A stepper motor, adjusted outside the box, rotates the whole instrument to control the elevation viewing angle. The spectrograph covers the range 292–436 nm and its entrance slit is 50 µm wide. A Sony ILX511 CCD (charged coupled device) detects the light in 2048 individual pixels. The whole spectrograph is cooled by a Peltier stage to guarantee a stable temperature of the optical setup and a small dark current signal. The measurement process and spectra recording are controlled by a PC using MiniMAX, a software package developed by Dr. Udo Frieß at the Institute of Environmental Physics, the University of Heidelberg.

The system was mounted on a bracket, fixed at the north edge of the building's roof, at an azimuth viewing direction towards the north (Fig. 1). The temperature of the spectrograph was set below the ambient temperature, typically maintained at −5 °C, 0 °C, or 5 °C (depending on season) for several months. The signal spectra of dark current and electronic offset were measured generally each month or whenever the working temperature of the instrument was changed. We used 10 000 msec and 1 scan for dark current measurements and 3 msec and 1000 scans for electronic offset measurements. Measurements were made at 3°, 6°, 10°, 20°, 30°, 45°, and 90° elevation angles consecutively, with an integration time of about one minute for each elevation angle. The lower elevation measurements have a large sensitivity to absorptions in the boundary layer, while the zenith measurements are used as background spectra to account for Fraunhofer structures and stratospheric absorption.

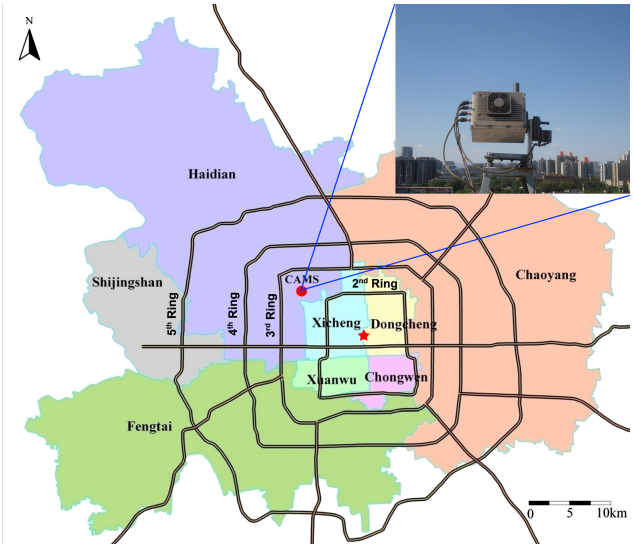

Fig. 1. A map of the Beijing city. The red dot indicates the CMA observation site, and the red star the position of Tian-An-Men, the center point of the city. A photo inside shows the surrounding environment of the instrument in the view direction (towards the north).

No strong emission sources were found around the building. The nearest road artery, called Zhongguancun South Street, is located in the west of the building (about 450 m). In the north, there is a playground in front of the observation building and some lower buildings nearby, and higher buildings are located far away, well below the lowest elevation angle view.

2.2 Spectral retrieval

The retrieval of NO_2 column densities is based on the DOAS method (Platt, 1994). The WinDOAS software (Fayt and Van Roozendael, 2001) was applied to analyze the spectra in the 400–420 nm window. Before the spectra are analyzed, the contribution of the dark current and electronic offset is removed using spectra measured at the same temperature. The logarithm of a Fraunhofer reference spectrum (FRS) as well as several trace gas absorption cross sections are fitted to the logarithm of each measured spectrum using a non-linear least squares fitting routine (allowing shift and squeeze of the fitted spectra). The FRS are selected among the measured spectra in such a way: first, they were measured during noon to minimize the stratospheric contribution; and second, they were measured at the 90° elevation angle to minimize the tropospheric contribution. One selected FRS can be used in the retrieval of the spectra measured typically during several days to a month. A low order polynomial, representing the slow varying contribution of broad-band absorption, as well as the Rayleigh and Mie-scattering processes, and a

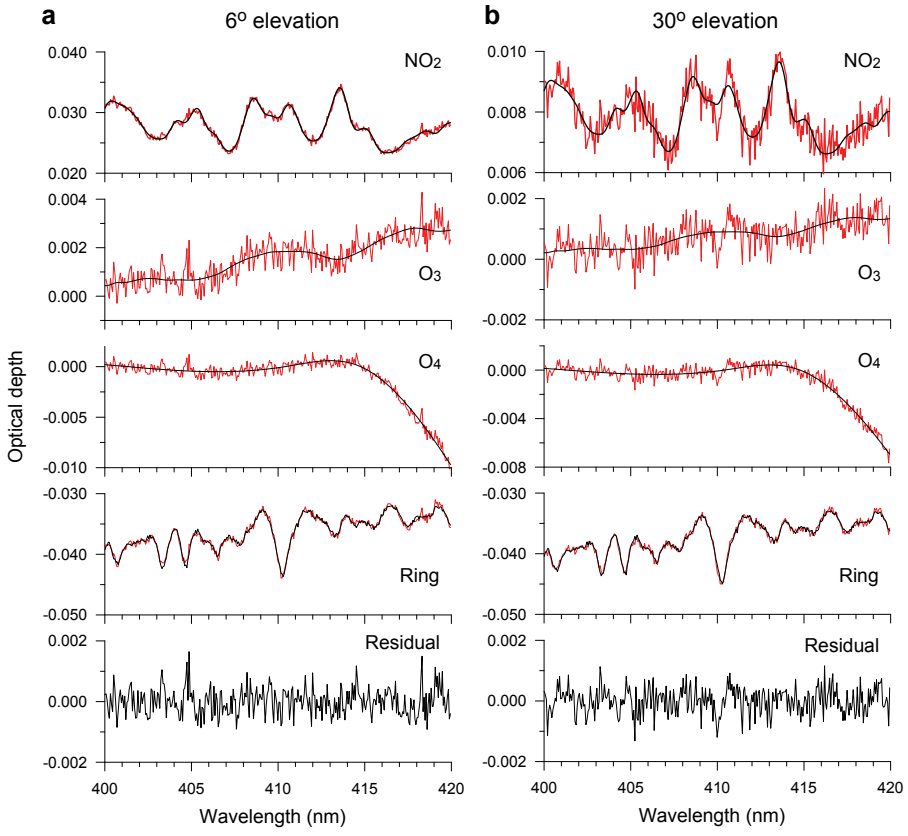

Fig. 2. Examples of the NO_2 retrieval for **(a)** high absorption (12 August 2008, 12:32 BJT, at 6° elevation angle, with NO_2 differential slant column density (DSCD) of 4.62×10^{16} molecules cm^{-2}) and **(b)** low absorption (12 August 2008, 12:35 BJT, at 30° elevation angle, with NO_2 DSCD of 1.31×10^{16} molecules cm^{-2}). The black lines indicate the reference spectra scaled to the respective absorptions (red lines) in the measured spectra. At the bottom, the spectral residual (difference between measured spectra and fit result) are shown.

Ring spectrum calculated by DOASIS (Kraus, 2001) were included. The cross sections of NO_2 at 294 K (Vandaele et al., 1998), O_3 at 221 K (Burrows et al., 1999a), and the oxygen dimmer O_4 at 298 K (Greenblatt et al., 1990) were taken into account. Figure 2 shows two examples of our spectral analysis, one for rather high NO_2 absorption for a measurement at low elevation angle, and one for rather low NO_2 absorption for a measurement at high elevation angle. The two spectra were taken around noon (Note that Beijing Time (BJT) equals Universal Time, Coordinated (UTC) plus 8 h). In both cases, the atmospheric NO_2 absorption structure can be clearly extracted from the measured spectra.

DOAS measurements using scattered sunlight yield the apparent (slant) column densities (SCD), which are defined as the trace gas concentrations integrated along the effective light path. The total SCD can be split into a tropospheric and a stratospheric part:

$$\mathrm{SCD} = \mathrm{SCD}_{\mathrm{trop}} + \mathrm{SCD}_{\mathrm{strat}} \,. \quad (1)$$

Considering the higher air density (more Rayleigh scattering) and higher particle loadings (more Mie scattering) in the lower atmosphere, it can be assumed that the last scattering event, before the light reaches the instrument, takes place in the lower troposphere. Thus it can be assumed that the light detected by the instrument traverses the same path in the stratosphere, independent of the telescope elevation angle α, i.e. $\mathrm{SCD}_{\alpha,\mathrm{strat}} \approx \mathrm{SCD}_{90,\mathrm{strat}}$. Since not only the measured spectra, but also the FRS contains atmospheric trace gas absorption, the result of the DOAS analysis represents the so-called differential slant column density (DSCD), which represents the difference in absorption between the atmospheric measurement and the FRS:

$$\mathrm{DSCD}_{\alpha} = \mathrm{SCD}_{\alpha} - \mathrm{SCD}_{\mathrm{FRS}}. \quad (2)$$

Tropospheric DSCDs ($\mathrm{DSCD}_{\mathrm{trop}}$) are produced by subtracting the DSCD of the zenith viewing direction, i.e. at 90° elevation angle, of the same elevation sequence from the respective DSCDs of the other viewing directions, e.g. at an elevation angle of α:

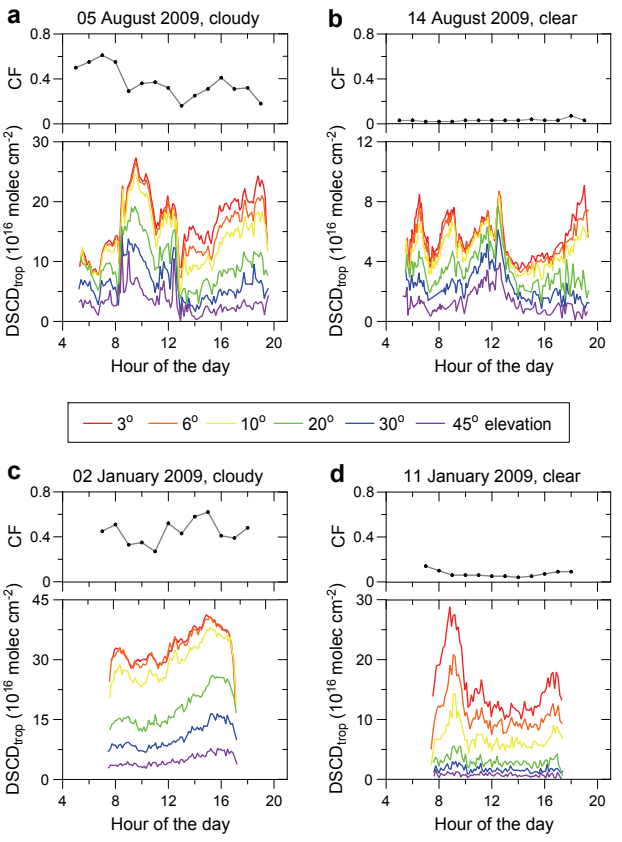

Fig. 3. Diurnal variations of the NO_2 tropospheric differential slant column density ($DSCD_{trop}$), measured from the MAX-DOAS, and the cloud fraction (CF) observed from the satellite FY-2D. The different sub-plots show examples for heavily polluted (**a** and **c**) and relatively clean (**b** and **d**) cases in Beijing during summer (**a** and **b**) and winter (**c** and **d**) periods, respectively. (Please note the different y-scales.)

$$\begin{aligned} DSCD_{\alpha,trop} &= DSCD_{\alpha} - DSCD_{90^\circ} \\ &= (SCD_{\alpha} - SCD_{FRS}) - (SCD_{90^\circ} - SCD_{FRS}) \\ &= SCD_{\alpha} - SCD_{90^\circ} \\ &= (SCD_{\alpha,strat} + SCD_{\alpha,trop}) - (SCD_{90^\circ,strat} + SCD_{90^\circ,trop}) \\ &= SCD_{\alpha,trop} - SCD_{90^\circ,trop}. \end{aligned} \quad (3)$$

Therefore, changing the elevation angle α only has an influence on the absorption signal caused by tropospheric absorbers (Hönninger et al., 2004).

Figure 3 shows the measured tropospheric DSCDs of NO_2 for selected summer (5 and 14 August 2009) and winter (2 and 11 January 2009) days. As expected, in general, the $DSCD_{trop}$ increased with decreasing elevation angle on all days. In most cases (except 11 January 2009), the differences in $DSCD_{trop}$ at lower elevation angles (e.g. 3° and 6°) are small, indicating either very high aerosol load or a rather constant NO_2 concentration within the boundary layer (or both). On 11 January 2009, the strong increase between the 3° and 6° elevation angles indicates that the highest NO_2 concentrations were located close to the surface. The diurnal variation patterns of $DSCD_{trop}$ at different elevation angles are generally similar during one day, indicating the high sensitivity of all elevation angles to NO_2 in the PBL. The diurnal variations of the cloud fraction (CF) observed by the Chinese geostationary meteorological satellite FY-2D are also shown in Fig. 3. On the cloudy days (5 August 2009 and 2 January 2009), similar absolute values and a similar splitting of the $DSCD_{trop}$ for different elevation angles are observed, indicating that most of the NO_2 was located below the cloud.

The tropospheric DSCDs of NO_2 are higher on heavily polluted days (5 August 2009 and 2 January 2009) than on less polluted days (14 August 2009 and 11 January 2009) during both summer and winter periods. Please note that in this study we focus on the retrieval of the tropospheric NO_2 VCD from observations at relatively high elevation angles (30° and 45°). A full profile retrieval of aerosols and trace gases from the MAX-DOAS observations using all observation angles will be the subject of a forthcoming publication.

2.3 Radiative transfer simulations

The SCD depends not only on the NO_2 concentration profile, but also on the effective length of the light path and the observation geometry and therefore needs to be converted to the vertical column density (VCD). The VCD does not depend on the light path and the observation geometry and can thus be used to compare different measurements. The air mass factor (AMF) in the troposphere is given by the ratio of the tropospheric SCD to VCD:

$$AMF_{\alpha,trop} = \frac{SCD_{\alpha,trop}}{VCD_{trop}}. \quad (4)$$

According to the above equation, the tropospheric SCDs at the elevation angles of α and 90° can be expressed as

$$SCD_{\alpha,trop} = VCD_{trop} \cdot AMF_{\alpha,trop} \quad (5)$$

$$SCD_{90,trop} = VCD_{trop} \cdot AMF_{90,trop}. \quad (6)$$

By substituting Eqs. (5) and (6) into Eq. (3), we obtain

$$VCD_{trop} = \frac{DSCD_{\alpha,trop}}{DAMF_{\alpha,trop}} \quad (7)$$

where the $DAMF_{\alpha,trop}$ is the differential tropospheric atmospheric air mass factor, i.e.

$$DAMF_{\alpha,trop} = AMF_{\alpha,trop} - AMF_{90,trop}. \quad (8)$$

If the trace gas layer is mainly located near the ground, e.g. in the PBL, the air mass factor can be expressed approximately as

$$AMF_{\alpha,trop} \approx \frac{1}{\sin(\alpha)}. \quad (9)$$

Table 1. Physical parameters used in the AMF calculations.

No.	Case name	Pollutant profile range (km)	Aerosol optical depth (τ)	Aerosol single scattering albedo (ω)	Aerosol asymmetry factor (g)	Surface albedo (alb)
1	ref	0–1.0	1.0	0.90	0.70	0.05
2	$\tau = 0.1$	0–1.0	0.1	0.90	0.70	0.05
3	$\tau = 2.0$	0–1.0	2.0	0.90	0.70	0.05
4	0–0.2 km	0–0.2	1.0	0.90	0.70	0.05
5	0–2.0 km	0–2.0	1.0	0.90	0.70	0.05
6	$\omega = 0.85$	0–1.0	1.0	0.85	0.70	0.05
7	$\omega = 0.95$	0–1.0	1.0	0.95	0.70	0.05
8	$g = 0.68$	0–1.0	1.0	0.90	0.68	0.05
9	alb = 0.10	0–1.0	1.0	0.90	0.70	0.10

Therefore, with $AMF_{90,trop} = 1$, Eq. (7) becomes

$$VCD_{trop} = \frac{\sin(\alpha) \cdot DSCD_{\alpha,trop}}{1-\sin(\alpha)}, (\alpha \neq 90^\circ). \quad (10)$$

Equation (10) is often referred to as geometric approximation for the calculation of tropospheric NO_2 VCDs (e.g. Brinksma et al., 2008). Here it should be noted that tropospheric NO_2 VCDs retrieved from MAX-DOAS observations at high elevation angles (30° and 45°) are sensitive for the lowest few kilometers (below about 5km) of the troposphere; the exact altitude range depends on aerosol and cloud conditions. In any case, the derived tropospheric VCD includes the NO_2 concentrations in the boundary layer.

To evaluate the accuracy of the geometric approximation, we calculated more exact tropospheric NO_2 AMFs at 417 nm over Beijing, using the 3-D fully spherical Monte Carlo atmospheric radiative transfer model (McArtim) (Deutschmann, 2009; Deutschmann et al., 2011). As shown in Table 1, various environmental conditions were taken into account in our McArtim simulations. The aerosol optical depth (τ) of 1.0, pollutant (NO_2 and aerosol) profile range of 0–1.0 km, aerosol single scattering albedo (ω) of 0.90, aerosol asymmetry factor (g) of 0.70, and surface albedo (alb) of 0.05 have been considered as reference case. Sensitivity tests were performed for other cases, where one of these parameter settings was changed to $\tau = 0.1$, $\tau = 2.0$, 0–0.2 km, 0–2.0 km, $\omega = 0.85$, $\omega = 0.95$, $g = 0.68$, and alb = 0.10, respectively. In the AMF calculation, the pollutant vertical profiles are a key parameter affecting the results. Aerosols were assumed to be located at the same altitude range as tropospheric NO_2, with optical parameters selected according to previous work (He et al., 2009; Wang et al., 2009; Clémer et al., 2010). The diurnal variations of the tropospheric NO_2 AMF as well as DAMF in different seasons were calculated. In these simulations the respective solar zenith angles and relative azimuth angles were taken into account.

In the following, the deviation of the tropospheric NO_2 VCD over Beijing determined by the geometric approximation, $VCD_{\sin\alpha}$, using Eq. (10) from the one calculated by Eq. (7) using the McArtim simulated AMF, VCD_{AMF}, is calculated from the ratios of the respective tropospheric DAMF:

$$\frac{VCD_{\sin\alpha}}{VCD_{AMF}} = \frac{\sin(\alpha) \cdot DAMF_{\alpha,trop}}{1-\sin(\alpha)} \quad (11)$$

In Figs. 4 and 5, the diurnal variations of the $VCD_{\sin\alpha}$ to VCD_{AMF} ratio for different seasons under various environmental conditions are shown. The results are presented for the two elevation angles used for the determination of the tropospheric NO_2 VCD, with $\alpha = 30^\circ$ in Fig. 3 and $\alpha = 45^\circ$ in Fig. 4, respectively. It can be seen that the biases caused by the simplification of using the geometric approximation are generally much smaller at $\alpha = 30^\circ$ than at $\alpha = 45^\circ$. In an absolute sense, the biases at $\alpha = 30^\circ$ are within 10 % in most cases, within 20 % in all cases, and the biases at $\alpha = 45^\circ$ are over 20 % during most of the daytime period. Thus in the following, the tropospheric NO_2 VCDs over Beijing retrieved by the geometric approximation at $\alpha = 30^\circ$ are used. Please note that the influence of elevated aerosol layers on both MAX-DOAS and satellite observations is discussed in Sect. 3.6.2.

2.4 Satellite data

For this study, we compared the SCIAMACHY and OMI tropospheric NO_2 VCDs with our ground-based MAX-DOAS measurements. Below only a brief introduction of the satellite instruments is given, and the readers are referred to published literature for a detailed description of SCIAMACHY (e.g. Bovensmann et al., 1999; Chen et al., 2009; Beirle et al., 2010) and OMI (e.g. Levelt et al., 2006; Boersma et al., 2007, 2011).

SCIAMACHY was launched onboard the ESA satellite ENVISAT in March 2002. It is an 8 channel spectrometer, and designed to measure the sunlight upwelling from the Earth's atmosphere in different viewing geometries in the UV to the NIR (240–2380 nm) with a spectral resolution of 0.22–1.48 nm. ENVISAT orbits the Earth in a Sun-synchronous orbit with an inclination from the equatorial

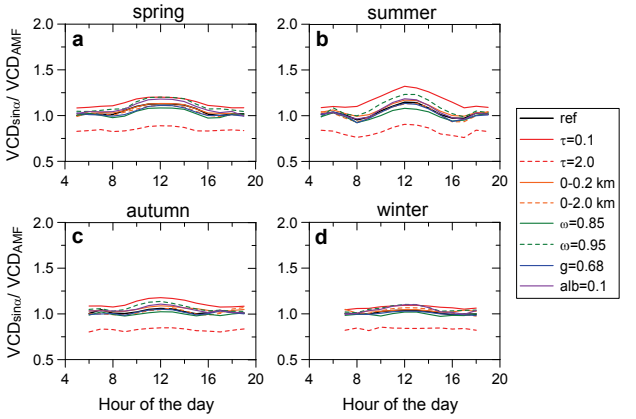

Fig. 4. Ratios of the tropospheric NO_2 VCD, calculated assuming the so-called geometric approximation ($VCD_{\sin\alpha}$), to those calculated using various AMFs as simulated by the radiative transfer model (VCD_{AMF}), for the 30° elevation angle in different seasons. Detailed descriptions of parameters used in the AMF calculations are given in Table 1.

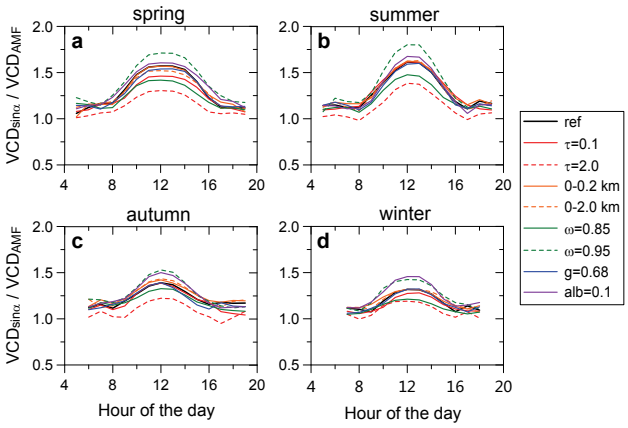

Fig. 5. Same as Fig. 4, but for the 45° elevation angle.

plane of 98.5°. It performs one orbit in approx. 100 min, with a local equator crossing time of about 10:00 a.m. LT. It is operated in different viewing geometries, including nadir, limb, and solar/lunar occultation. In nadir geometry (i.e. directed (almost) vertically down to the Earth's surface), the instrument performs an across-track scan of about ±32°, equivalent to a swath width of 960 km. The footprint of a single nadir observation is typically $30 \times 60\,km^2$. Global cover of nadir measurements is achieved after 6 days. Here tropospheric NO_2 columns are used which were retrieved at MPI for Chemistry in the spectral window between 430–450 nm (channel 3). The retrieval uses stratospheric profiles from SCIAMACHY limb measurements to estimate the stratospheric column (Beirle et al., 2010). Tropospheric AMFs are calculated for a globally unique, simple profile, i.e. 80 % of tropospheric NO_2 within a 1 km deep boundary layer. A slightly different standard profile with 95 % of tropospheric NO_2 in the PBL (hereafter referred as std95 profile) is also used for the retrieval of tropospheric NO_2 over severely polluted urban areas, such as Beijing in this study. Details can be found in the work of Chen et al. (2009) and Beirle and Wagner (2010).

OMI flying on NASA's EOS Aura satellite is a nadir-viewing imaging spectrograph that measures direct and atmosphere-backscattered sunlight in the UV-VIS range from 270 nm to 500 nm with a spectral resolution of about 0.5 nm. OMI has three spectral channels, and slant columns of NO_2 are retrieved in the 405–465 nm spectral window (Boersma et al., 2007, 2011). EOS Aura was launched on 15 July 2004 and traces a Sun-synchronous, polar orbit at approximately 705 km altitude with a period of 100 min and a local equator crossing time between 13:40 and 13:50. OMI's field of view corresponds to a 2600 km wide spatial swath on the Earth's surface for one orbit, large enough to achieve complete global coverage in one day. Its spatial resolution is $24 \times 13\,km^2$ in nadir, and increases to $68 \times 14\,km^2$ at the swath edges (discarding the outer 5 pixels). Compared to SCIAMACHY, OMI has a better spatial resolution and by far more measurements. In this study, OMI NO_2 tropospheric VCDs from TEMIS (Tropospheric Emission Monitoring Internet Service, at http://www.temis.nl), developed within the project "Derivation of Ozone Monitoring Instrument tropospheric NO_2 in near-real time" (DOMINO), are used (DOMINO versions 1.02 and 2.0). For the DOMINO retrievals, the stratospheric NO_2 column is assimilated by the TM4 chemical transport model. Tropospheric AMFs are calculated based on tropospheric a priori profiles of NO_2 from TM4. In version DOMINO v2.0, some improvements (radiative transfer calculations, a priori terrain heights and surface albedo, and the TM4 sampling) have been introduced to this last step. For details see Boersma et al. (2007, 2011).

Due to the different sampling time, spatial resolution, and a priori assumptions of the retrievals, differences of the satellite products are expected.

3 Results and discussions

3.1 Time series of bimonthly mean NO_2 VCD

Figure 6 presents the time series of the tropospheric NO_2 VCD over Beijing from August 2008 to September 2011. Only the data measured between 08:00 and 17:00 BJT, corresponding to the sunshine period during the wintertime, have been taken into account. Since the measurements were interrupted irregularly due to various problems, e.g. power supply breaking and fan replacement (shipped back to Germany during 8 June–17 July 2009), insufficient data are available for some months. Therefore, the data have been grouped into two-month intervals to increase the statistical significance. The annual cycles of the mean and median tropospheric NO_2

VCDs are clearly obvious, with the maxima occurring in winter and the minima in summer. Such an annual variation pattern is in accordance with in situ NO_2 surface measurements in Beijing (Jiang et al., 2006), as well as in other cities, e.g. in Leicester, United Kingdom (Kramer et al., 2008). Here it is interesting to note that in several existing studies, the seasonal variation measured from satellite shows a systematically higher amplitude (e.g. Richter et al., 2005). Possible reasons for this discrepancy might be the specific sampling time of the satellite measurements and also the strong influence of aerosols on the satellite's sensitivity for the boundary layer, see below.

The average, median, minimum and maximum values of the tropospheric NO_2 VCDs over Beijing in winter (12–02) and summer (06–08) months from 2008 to 2009 are summarized in Table 2. The daily mean tropospheric NO_2 VCDs over Beijing varied from 0.5 to 13.3 with an average of 3.6 during summertime, and from 0.2 to 16.8 with an average of 5.8 during wintertime, in units of 10^{16} molecules cm^{-2}. It is interesting to note that also the maxima as well as the 75th and 90th percentiles of the bimonthly (but also monthly) data show the same systematic annual variation (Fig. 6). In contrast, the annual variations of the lower percentile and minimum values do not show a similar seasonal pattern. Note that the variability of the tropospheric NO_2 VCD over Beijing is much higher during wintertime than during summertime. When the weather system is very stable, a larger amount of NO_2 accumulate near the sources in winter than in summer due to higher emissions and slower photolysis of NO_2 in winter. On the other hand, the weather system can be very unstable sometimes, with much stronger winds in winter, leading to very low NO_2 concentrations in winter, as compared to summer.

3.2 Seasonal and diurnal variations

Figure 7 shows the average diurnal variations of the tropospheric NO_2 VCD in different seasons from August 2008 to September 2011, and Table 3 gives the values at selected times of the day. Although the diurnal variation patterns of NO_x emissions in Beijing appear to be the same in different seasons, the diurnal variation patterns of tropospheric NO_2 are rather different from one season to another, owing to the differences in its emission strength and atmospheric lifetime. In addition, the dynamic processes associated with the PBL structure might influence the accumulation and dispersion of NO_2. Note that in contrast to the NO_2 volume mixing at the surface, the NO_2 VCD should not change directly with a variation in the PBL height. As shown in the figure, the VCD maximum occurred in the late morning during summer (4.8×10^{16} molecules cm^{-2} at 11:00 BJT), and in the late afternoon during winter (7.0×10^{16} molecules cm^{-2} at 17:00 BJT). The largest difference between the VCDs of different seasons took place in the afternoon, for example, the tropospheric NO_2 VCD at 16:00 BJT was 4.1×10^{16} molecules cm^{-2} higher in winter (6.9×10^{16} molecules cm^{-2}) than in summer (2.8×10^{16} molecules cm^{-2}). The differences in the tropospheric NO_2 VCD among the seasons were much smaller in the morning, with a maximum of 1.6×10^{16} molecules cm^{-2} at 08:00 BJT and a minimum ranging 0.1 to 0.5×10^{16} molecules cm^{-2} at 11:00 BJT. These are probably caused by the complex interplay of the emission, chemistry and transport, with generally higher emission rates, longer NO_2 lifetime and less dispersion efficiency in winter. Our results also indicate that the seasonal variation pattern of tropospheric NO_2 retrieved by the satellites with different overpass time can be different to some extent. For example, OMI, which has an overpass time in the early afternoon, should get a more pronounced seasonal variation than SCIAMACHY, which has an overpass time in the late morning. It should be noted that, in recent comparisons of the seasonal cycle of the tropospheric NO_2 VCD from different satellite instruments (Richter et al., 2008), very similar amplitudes of the seasonal cycle above China are found. However, this might be caused by the fact that these studies used monthly average values over rather large areas, which include many cities and surrounding areas, and for which the effect of the diurnal cycle should be largely smeared out.

3.3 Weekly cycle

Beirle et al. (2003) investigated the weekly cycle of tropospheric NO_2 VCDs using the GOME satellite data of 1996–2001. They found a clear Sunday minimum of tropospheric NO_2 VCD in the cycles of the industrialized regions and cities in the US, Europe and Japan, with the Sunday NO_2 VCDs being about 25–50 % lower than working day levels. However, no weekend effect was found in the cities of China, including Beijing (Beirle et al., 2003; Hayn et al., 2009). A similar result was also reported for the city of Leicester, United Kingdom (Kramer et al., 2008). For this study we investigated the weekly cycle of the tropospheric NO_2 VCD for Beijing by our ground-based MAX-DOAS measurements. Figure 8 shows the average weekly cycle of the daily mean tropospheric NO_2 VCD over Beijing from August 2008 to September 2011. The weekly cycle of daily mean NO_2 over Beijing was not very pronounced, though a Wednesday maximum (with a mean value of 4.8×10^{16} molecules cm^{-2}) and a Sunday minimum (with a mean value of 4.0×10^{16} molecules cm^{-2}) can be seen. Figure 9 shows the weekly cycle of the diurnal variation in tropospheric NO_2 VCD over Beijing. One unexpected finding was that in the morning, the tropospheric NO_2 VCD was much higher on Wednesday than on the rest days of the week. Here it should be noted that this Wednesday maximum is found not only if all data are considered, but also for averages of individual seasons or years. The NO_2 VCD on Saturday was also high from the late morning to the late afternoon, being the largest (5.3×10^{16} molecules cm^{-2}) at 17:00 BJT.

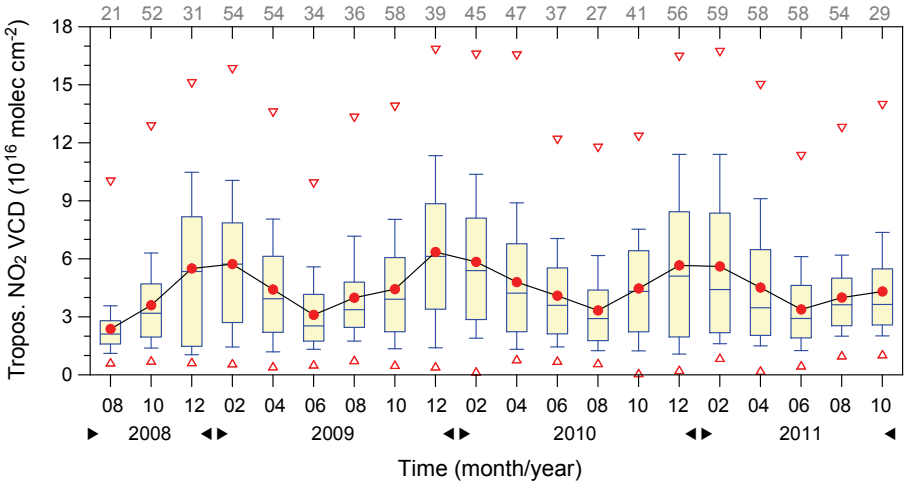

Fig. 6. Time series of the tropospheric NO_2 vertical column density (VCD) over Beijing from August 2008 to September 2011. Given are the bimonthly mean values for each two sequential months between August 2008 and August 2011. Lower (upper) error bars, yellow boxes and lower (upper) triangles are 10th (90th), 25th (75th) percentiles and minimums (maximums) of the data grouped in each interval, respectively. Hyphens inside the boxes are the medians, and red circles the mean values. The numbers of integrated sampling days for each data point are labeled at the top axis.

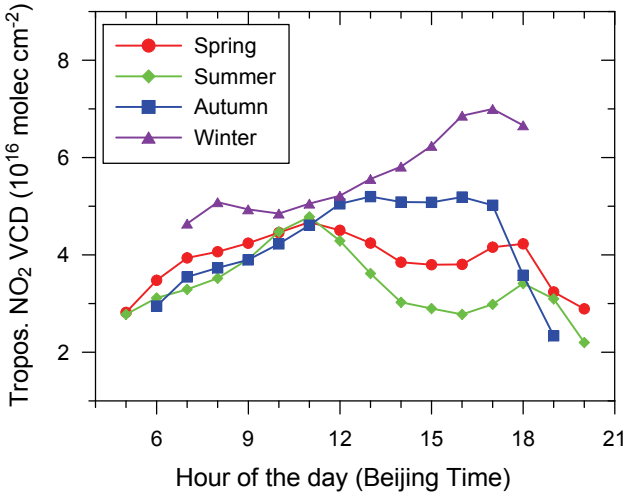

Fig. 7. Diurnal variations of the tropospheric NO_2 VCD, averaged for different seasons from August 2008 to September 2011.

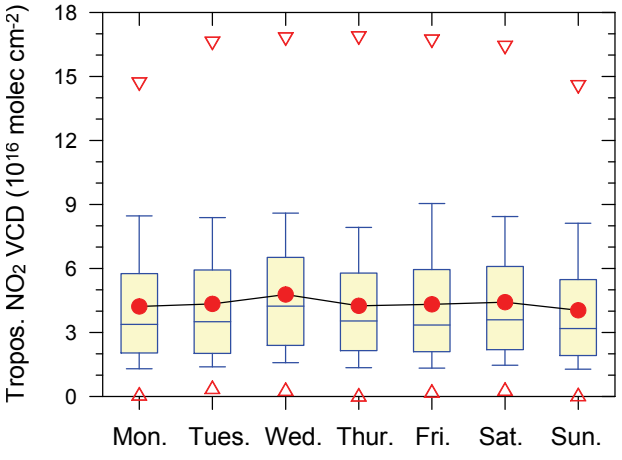

Fig. 8. Weekly cycle of the daily mean tropospheric NO_2 VCD, averaged over the period of August 2008 to September 2011.

Apparently, the tropospheric NO_2 VCD over Beijing was the lowest on Sunday late afternoon (4.3×10^{16} molecules cm^{-2} at 17:00 BJT).

The industrial and traffic activities are the main NO_x sources in Beijing, contributing to the NO_x over Beijing by about 30 % and 70 %, respectively (Ma et al., 2012; Zhao et al., 2012). The industrial source emissions in Beijing and its surrounding areas appear not to take a significant weekly cycle. Since 11 October 2008, new traffic restrictions have been implemented in Beijing. Each vehicle is not allowed to travel on the roads during one of the five working days (weekdays, i.e. Monday to Friday), specified according to its license plate number. However, there have been no travel limitations on weekends (Saturday and Sunday) and festival days. The data obtained during the festival days, which can be either on weekdays or weekends, were not taken into account in our statistics. The social activities and living habits in China are different from western countries, and heavy traffic in Beijing, even on Saturday, has been a well-known phenomenon. At present, we have no social statistic data to explain the Wednesday maximum feature. Anyway, in contrary to previous work of Beirle et al. (2003), we found apparent indications for the weekday and weekend effects on the tropospheric NO_2 VCD over Beijing. Note that the period (1996–2001) investigated by Beirle et al. (2003) and Hayn

Table 2. Tropospheric NO_2 VCDs (in units of 10^{16} molecules cm^{-2}) over Beijing in winter and summer months from 2008 to 2011.

	Winter 2008–2009	Summer 2009	Winter 2009–2010	Summer 2010	Winter 2010–2011	Summer 2011
Average	5.6	3.5	6.1	3.7	5.6	3.7
Median	5.5	2.9	5.7	3.2	4.8	3.3
Minimum	0.6	0.6	0.2	0.6	0.3	0.5
Maximum	15.8	13.3	16.8	12.1	16.7	12.8

Table 3. Average tropospheric NO_2 VCDs (in units of 10^{16} molecules cm^{-2}) over Beijing for different times of the day and different seasons.

Beijing Time	Spring	Summer	Autumn	Winter
08:00	4.1	3.5	3.7	5.1
11:00	4.7	4.8	4.6	5.1
14:00	3.8	3.1	5.1	5.8
17:00	4.2	3.0	5.0	7.0

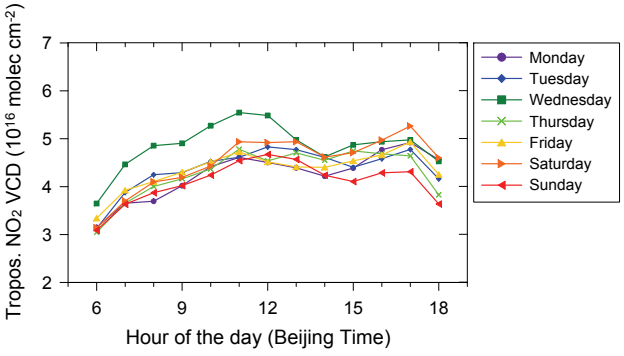

Fig. 9. Diurnal variations of the tropospheric NO_2 VCD for different days of the week, averaged over the period of August 2008 to September 2011.

et al. (2009) was about 10 yr earlier than the measurement period (2008–2011) of this study. There could be a large change in emission source structure and living activities between the two periods. Moreover, Beirle et al. (2003) and Hayn et al. (2009) used the data from the GOME satellite, which (a) has an overpass time of around 10:30 BJT for Beijing, and the weekend effect might not be so significant at this time as in the afternoon and (b) has large ground pixels of $320 \times 40\,km^2$, i.e. the weekly patterns for Beijing are in fact regional averages.

3.4 Olympic Games effect

Beijing implemented strict control measures, including the restrictions of both traffic and industrial emissions in the city and its surroundings, to ensure good air quality for the 2008 Olympic Games. It has been estimated that the daily emissions of primary pollutants were reduced significantly, e.g. by 47 % for NO_x (with 30 % from traffic restrictions), during the Games (Wang et al., 2010a). Satellite measurements have revealed that the tropospheric NO_2 over Beijing was reduced by about 40–60 % during the 2008 Olympic Games (Mijling et al., 2009; Witte et al., 2009; Yu et al., 2010). Note that these results were based on the comparisons of August 2008 (some including September 2008) with the previous month, or with the same month in the previous year. Our MAX-DOAS measurements started on 6 August 2008, just two days before the opening of the Beijing 2008 Olympic Games. Though no data are available before August 2008, we can make an evaluation of the post- Olympic Games effect through our measurements.

Figure 10 presents the monthly averaged diurnal variations of the tropospheric NO_2 VCD over Beijing for August in the years of 2008, 2009, 2010 and 2011. It is shown clearly that the tropospheric NO_2 VCDs were much smaller in 2008 than in other years, especially in the morning and early afternoon. The most significant difference occurred at 11:00 BJT, when the daily maximum of the tropospheric NO_2 VCDs took place in each year. In the late afternoon, the effects of the emission control measures are much less obvious in the NO_2 VCDs. Table 4 lists the tropospheric NO_2 VCD values at selected times of the day in August, as well as the relative reductions (in percent) of the 2008 values compared to 2009, 2010 and 2011, respectively. Based on our measurements in the morning and early afternoon, the decreases in the tropospheric NO_2 VCD over Beijing during the 2008 Olympic Games are estimated to be 39–54 %, with respect to the following years of 2009, 2010 and 2011, respectively. Note that the VCDs were slightly lower in 2010 than in 2009 and 2011. While the NO_x emissions seems not to be lower in 2010 than in 2009 and 2011, as indicated by the summer time tropospheric NO_2 VCD values from 2009 to 2011 (Table 2), this reduction might be due to the variability of the meteorological conditions; also the measurements were interrupted for some days (e.g. 10–15 August 2010). Our evaluation on the control measure effects is generally in agreement with the previous estimates based on satellite measurements during the 2008 Olympic Games and before (Mijling et al., 2009; Witte et al., 2009; Yu et al., 2010).

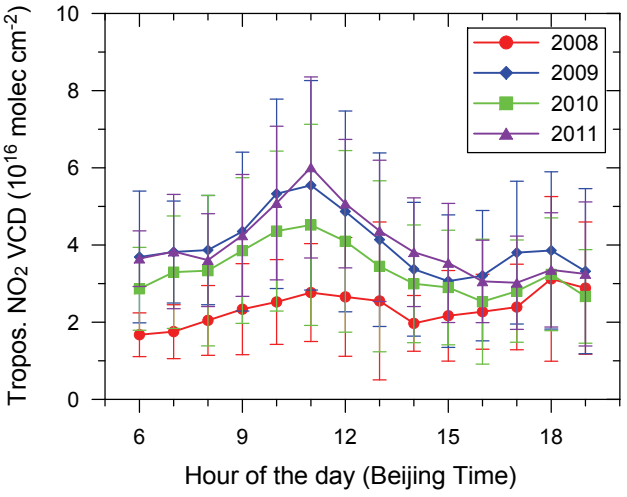

Fig. 10. Diurnal variations of the tropospheric NO_2 VCD in August for the years of 2008, 2009, 2010 and 2011. The bars refer to the standard deviations.

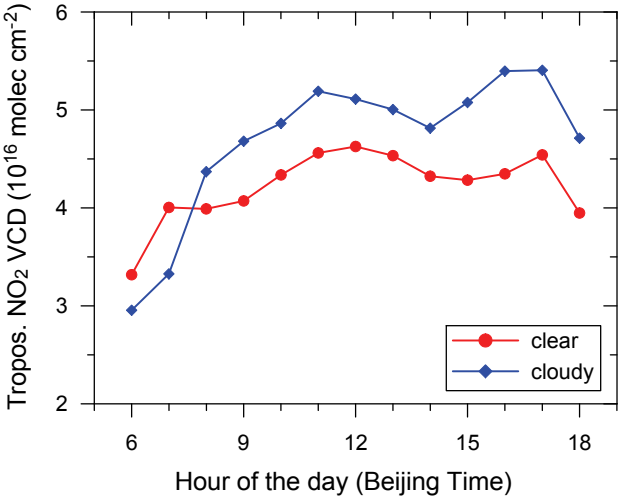

Fig. 11. Diurnal variations of the tropospheric NO_2 VCD under clear and cloudy conditions, averaged over the period of August 2008 to September 2011.

3.5 Cloud effect

Since most of tropospheric NO_2 is located well below clouds, especially in urban areas, satellite observations of the tropospheric NO_2 VCDs are restricted mainly to cloud-free conditions. In contrast, ground-based MAX-DOAS instruments can measure the tropospheric NO_2 VCDs under both clear and cloudy conditions with almost similar sensitivity. Figure 11 shows the average diurnal variations of the tropospheric NO_2 VCD under both clear and cloudy conditions from August 2008 to September 2011. The cloud fraction (CF) observed by the Chinese geostationary meteorological satellite FY-2D was applied to determine mostly clear ($CF < 0.3$) or mostly cloudy ($CF > 0.3$) condition. During 09:00–18:00 BJT, the differences in the tropospheric NO_2 VCD between the clear and cloudy conditions are typically $0.5–0.8 \times 10^{16}$ molecules cm^{-2}, with an increase of 12–14 % from the clear to cloudy condition. While we cannot rule out a remaining cloud effect on the retrieval of the tropospheric NO_2 VCD from the MAX-DOAS observations, this difference is probably caused by the effect of clouds on the tropospheric photochemistry: below the cloud, the loss rate of NO_2 by photolysis becomes lower due to less solar radiation. Note that there was an exception in the early morning, when the tropospheric NO_2 VCD was higher under the clear condition. Currently we have no explanation for this finding.

Additional scattering on cloud particles changes the color of the sky. On clear days the sunlight is mainly scattered on air molecules (Rayleigh scattering), which shows a strong wavelength dependence (proportional to λ^{-4}) causing the blue color of the sky. In the presence of clouds, the probability of the light observed by the MAX-DOAS instrument to be scattered by cloud particles is strongly increased. Since these scattering events show almost no wavelength dependence, the relative light intensity at large wavelengths is strongly increased compared to cloud-free conditions. Thus the presence of clouds can be identified by a so-called color ratio (e.g. Sarkissian et al., 1994; Wagner et al., 2009), which in our study is defined as the ratio of the intensity at 320 nm (C320) to that at 434 nm (C434). In Fig. 12 this color ratio is shown as a function of solar zenith angle (SZA) for clear and cloudy conditions, averaged for the period from August 2008 to September 2011. Again, information about the cloud cover is taken from satellite observations. The effect of clouds on the C320/C434 ratio is clearly visible at solar zenith angles smaller than around 75°. Figure 13 presents the average diurnal variations of the C320/C434 ratio under clear and cloudy conditions for different seasons from August 2008 to September 2011. The role of the solar zenith angle can be seen from the diurnal variations of the C320/C434 ratio in different seasons. This indicates that it is possible to use the C320/C434 ratio, measured by MAX-DOAS itself, as a threshold parameter to separate clear and cloudy conditions. Our measurement data reveal that the tropospheric NO_2 VCD is correlated with the reciprocal of the C320/C434

Table 4. Average tropospheric NO_2 VCDs (in units of 10^{16} molecules cm^{-2}) in August from 2008 to 2011 for different times of the day. Given in parenthesis are the respective reductions of the 2008 values compared to the specified years.

Beijing Time	2008	2009	2010	2011
08:00	2.04	3.86 (47 %)	3.33 (39 %)	3.60 (43 %)
11:00	2.76	5.54 (50 %)	4.52 (39 %)	6.01 (54 %)
14:00	1.97	3.37 (42 %)	2.99 (42 %)	3.81 (48 %)
17:00	2.39	3.80 (37 %)	2.80 (15 %)	3.02 (21 %)

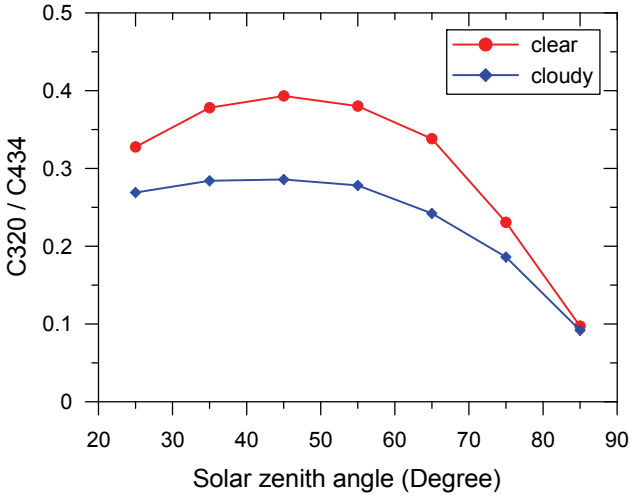

Fig. 12. Measured intensity ratio for wavelength of 320 nm (C320) and 434 nm (C434) as a function of solar zenith angle under clear and cloudy conditions, averaged over the period of August 2008 to September 2011.

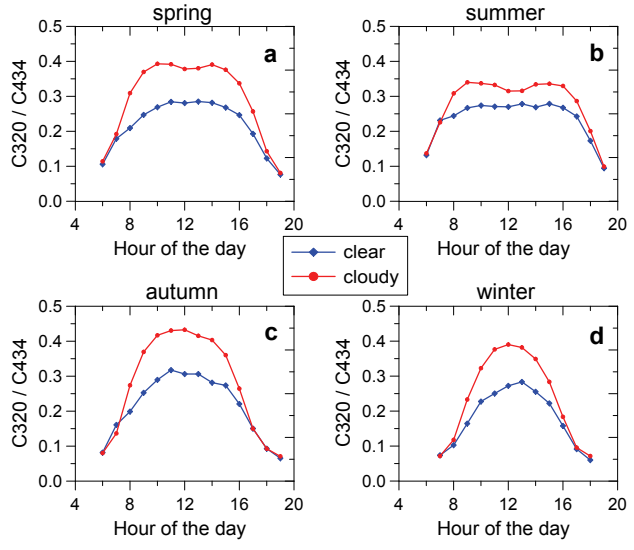

Fig. 13. Diurnal variations of the C320/C434 ratio under clear and cloudy conditions, averaged for different seasons from August 2008 to September 2011.

ratio, with a correlation coefficient of about 0.5 (not shown), confirming the results shown in Figs. 11 and 12.

3.6 Comparison with satellite data

We compared the tropospheric NO_2 VCDs derived by our ground based MAX-DOAS measurements to SCIAMACHY and OMI satellite data. One-hour average tropospheric NO_2 VCDs from MAX-DOAS measurements during 10:15–11:15 BJT and 13:00–14:00 BJT were used for the comparisons, corresponding to the overpass time of SCIAMACHY

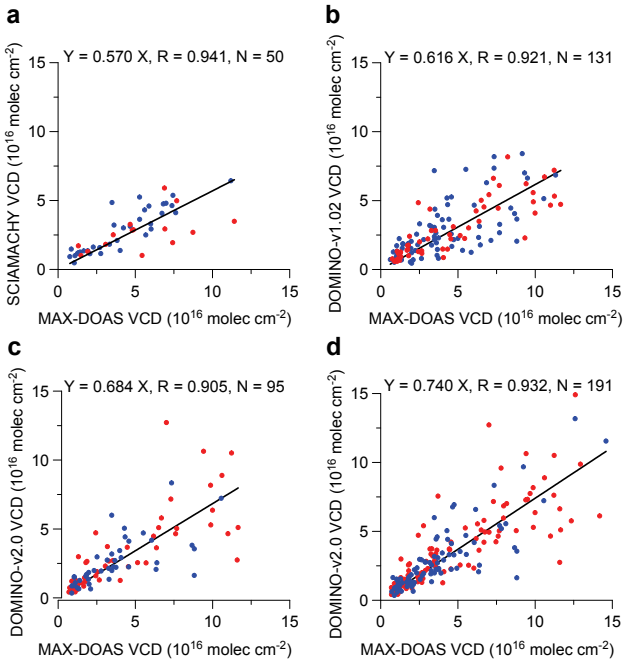

Fig. 14. Correlation of the hourly averaged tropospheric NO_2 VCDs over Beijing measured by ground-based MAX-DOAS with **(a)** coincident SCIAMACHY satellite data (2008–2010), **(b)** coincident OMI satellite data (DOMINO v1.02, 2008–2009), **(c)** coincident OMI satellite data (DOMINO v2.0, 2008–2009), and **(d)** coincident OMI satellite data (DOMINO v2.0, 2008–2011). Only data for days with CF < 0.3 are considered. Shown are regression results derived by combining the CTH < 1 km (red points) and CTH > 1 km (blue points) data together. The equation, $Y = k \cdot X$, was used for regressions, with k for slopes, R for correlation coefficients, and N for sampling numbers. Results for separate correlation analyses for CTH < 1 km and CHT > 1 km are shown in Table 5.

(around 10:45 BJT) and OMI (13:30 BJT) over Beijing, respectively. Using the average value over a relatively short period (e.g. one hour) for MAX-DOAS data limits the influence of the diurnal variation, which cannot be resolved by the satellite observations. The effective cloud fractions (CF) and cloud top heights (CTH) are taken from TEMIS for both SCIAMACHY and OMI retrievals. The satellite observations with CF > 0.3 were excluded from the comparison. Only the measurements with the satellite ground pixels containing the Beijing urban center (39.9° N, 116.4° E) were included for comparison, with a distance less than 0.2° latitude and 0.3° longitude for SCIAMACHY and 0.1° latitude and 0.2° longitude for OMI. For OMI, the measurements from the large outermost pixels (e.g. pixel numbers 1–10 and 51–60) or pixels where a "raw anomaly" had been reported (see http://www.temis.nl/docs/omi_warning.html) were skipped before the comparison. For SCIAMACHY, a dataset retrieved at MPI for Chemistry was used assuming a fixed relative tropospheric NO_2 profile. While in the standard retrieval, 80 % of the tropospheric NO_2 VCD is assumed to be in the PBL

(1 km high, constant concentration), and 20 % above (exponential decrease), here we used a slightly different profile with 95 % of tropospheric NO_2 in the PBL (the std95 profile), which probably better fits the true NO_2 profile close to strong pollution sources (Chen et al., 2009; Beirle, 2010). The results of this modified retrieval are typically 10–20 % larger than those of the standard retrieval. For OMI we used the two versions of DOMINO dataset, i.e. DOMINO v1.02 and DOMINO v2.0, from the TEMIS data base (Boersma et al., 2004, 2011).

In Fig. 14, we show scatter plots of the hourly averaged tropospheric NO_2 VCDs over Beijing measured by the ground-based MAX-DOAS with the 2008–2010 SCIAMACHY satellite data (Fig. 14a), with the 2008–2009 OMI satellite data (DOMINO v1.02) (Fig. 14b), with the 2008–2009 OMI satellite data (DOMINO v2.0) (Fig. 14c), and with the 2008–2011 OMI satellite data (DOMINO v2.0) (Fig. 14d). Both the OMI and SCIAMACHY data show good correlation with the ground measurements, with a slightly higher correlation coefficient for SCIAMACHY ($R = 0.94$) than for OMI ($R = 0.91$–0.93). The correlation coefficients between ground and satellite measured tropospheric NO_2 VCDs are higher than the ones found in previous studies, e.g. for the cities of Leicester and Shanghai, the latter having the R values of 0.6–0.7 (Kramer et al., 2008; Chen et al., 2009). The ratios of the average tropospheric NO_2 VCD from MAX-DOAS measurements to those from SCIAMACHY and OMI data are 1.75 and 1.35–1.62, respectively. In other words, the satellite observations underestimate the tropospheric NO_2 VCDs over Beijing systematically, by 43 % for SCIAMACHY and by 26–38 % for OMI, compared with the MAX-DOAS measurements. For the same period (2008–2009), such an underestimation is a little bit less for DOMINO v2.0 (32 %, Fig. 14c) than for DOMINO v1.02 (38 %, Fig. 14b), though the latter (v1.02) has slightly better correction with MAX-DOAS measurements than the former (v2.0). Using a longer period of dataset (2008–2011), the comparison with DOMINO v2.0 improves, with the underestimation decreasing to 26 % (Fig. 14d).

We also investigated the effect of low clouds on the correlation of our MAX-DOAS measurements with coincident satellite data. In contrast to clouds above the trace gas layer, which generally have a shielding effect, low clouds might even increase the sensitivity of the satellite observations for tropospheric NO_2 due to multiple scattering. Here it is important to note that especially measurements with high aerosol optical depth might be classified as cloudy measurements with low CTH.

In the SCIAMACHY retrieval, AMFs are calculated for clouds with a geometrical thickness of 1 km (Beirle and Wagner, 2010). Thus, the regular AMF calculation scheme for cloudy pixels cannot be applied for CTH < 1 km. For these situations, the cloud-free AMFs are used, arguing that such situations might be caused by aerosols, and accompanied by the warning to use these measurements with care (Beirle and Wagner, 2010). Therefore, we investigate the correlations separately for CTH below and above 1 km. The correlation results for either CTH > 1 km or CTH < 1 km are shown in Table 5. For SCIAMACHY, the correlation is better for the measurements with CTH > 1 km than with CTH < 1 km, in agreement with analysis results for Shanghai (Chen et al., 2009). For OMI, however, only small differences are found.

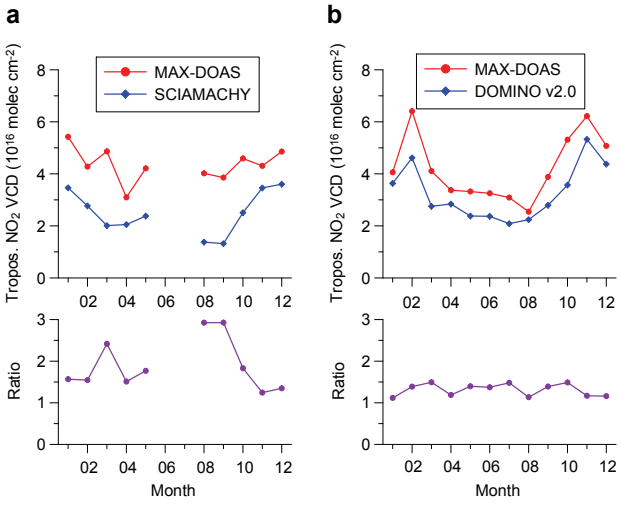

Fig. 15. Comparisons of the seasonal variation in the tropospheric NO_2 VCD over Beijing measured by ground-based MAX-DOAS with **(a)** coincident SCIAMACHY satellite data (2008–2010) and **(b)** coincident OMI satellite data (DOMINO v2.0, 2008–2011). Both the absolute VCD values from MAX-DOAS and satellite measurements (top) and their ratios (bottom) are shown.

Figure 15 presents the seasonal variation of the tropospheric NO_2 VCD over Beijing measured by the ground-based MAX-DOAS in comparison with coincident 2008–2010 SCIAMACHY and 2008–2011 OMI observations. The temporal patterns retrieved from satellite are generally in agreement with the MAX-DOAS results (note that some months have been skipped due to insufficient number of satellite data). The seasonal variation observed by OMI is much more pronounced than by SCIAMACHY, most probably due to the different overpass times: As shown in Fig. 7, for the overpass time of SCIAMACHY (around 10:45 BJT) the seasonal differences observed by MAX-DOAS are found to be much smaller than for the OMI overpass time (around 13:30 BJT). The larger variation of the SCIAMACHY time series is caused by the much smaller number of observations (typically 4–10 days each month) compared to OMI (7–21 days each month). The "monthly mean" tropospheric NO_2 VCDs measured by MAX-DOAS are typically 1.2–2.9 times as large as those retrieved by SCIAMACHY, and 1.1–1.5 times as large as those retrieved by DOMINO v2.0. There appears no seasonal dependence for such overestimation for OMI (DOMINO v2.0). However, the deviations appear to be highest in summer for SCIAMACHY, though the number

Table 5. Regression results using the MAX-DOAS measurement data versus coincident SCIAMACHY and OMI satellite data (DOMINO v1.02 and v2.0) for various cloud top height (CTH) conditions, as shown in Fig. 14.

Condition	CTH >1 km		CTH <1 km		All data	
	Slope	R	Slope	R	Slope	R
SCIAMACHY (2008–2010)	0.649	0.971	0.453	0.909	0.570	0.941
DOMINO v1.02 (2008–2009)	0.634	0.899	0.581	0.943	0.616	0.921
DOMINO v2.0 (2008–2009)	0.638	0.901	0.707	0.908	0.684	0.905
DOMINO v2.0 (2008–2011)	0.761	0.936	0.730	0.929	0.740	0.932

Table 6. Smoothing factors, i.e. the ratio of "true" and smoothed NO_2 VCD at the measurement site, estimated for OMI (for $26 \times 13\,km^2$ and $40 \times 13\,km^2$ pixel size) and SCIAMACHY (for 60×30 km^2 pixel size) resolution, using multi-year seasonal mean OMI VCDs and nighttime lights as proxy for the "true" NO_2 distribution.

Satellite resolution	OMI proxy				Nighttime
	Spring	Summer	Autumn	Winter	light proxy
OMI $26 \times 13\,km^2$	1.09	1.14	1.04	1.00	1.11
OMI $40 \times 13\,km^2$	1.15	1.21	1.08	1.03	1.26
SCIA $60 \times 30\,km^2$	1.34	1.46	1.21	1.14	1.75

of data used in the statistics might be insufficient. Possible reasons for these differences are discussed in the next subsections.

3.6.1 Gradient smoothing effect

An underestimation of the tropospheric NO_2 VCDs by satellite observations over urban areas has been reported previously. Chen et al. (2009) showed that tropospheric NO_2 VCDs from zenith-sky measurements in Shanghai are about 2 times as large as those retrieved from SCIAMACHY data. By comparing the spatial distributions of NO_2 and nighttime light pollution around Shanghai, they demonstrated that the lower VCDs from satellite are partly caused by the strong spatial gradients of NO_2 around megacities, which are not resolved by the satellite observations (Chen et al., 2009).

Here we perform a similar study to evaluate how far the higher MAX-DOAS VCDs in Beijing, compared to SCIAMACHY and OMI satellite products, can be explained by the "smoothing" of spatial patterns due to the large satellite ground pixels. For this purpose, we simulate the smoothing of the NO_2 spatial distribution for different satellite ground pixel sizes.

We use different proxies for the "true" spatial gradient of the NO_2 distribution:

1. As one extreme, we take the distribution of nighttime lights (Cinzano et al., 2001), as in Chen et al. (2009), with high spatial resolution (0°0′30″, here downscaled to 0.1°). This is rather a proxy of the emissions instead of column densities, i.e. spatial gradients are probably overestimated, and thus this proxy can be considered as an upper limit for the smoothing effect.
2. Second, we take the long-term mean NO_2 distribution derived from OMI as proxy for the NO_2 distribution. The OMI mean is already limited by the OMI spatial resolution, i.e. spatial gradients are already smeared out; thus, this proxy gives only a lower limit for the smoothing effect. Due to the long time series of OMI measurements, seasonal means can be considered, i.e. the seasonality of the smoothing effect can be evaluated.

For these proxies, mean synthetic "satellite maps" are generated for satellite footprints of $26 \times 13\,km^2$, $40 \times 13\,km^2$ (for OMI) and $60 \times 30\,km^2$ (for SCIAMACHY). This procedure is illustrated in Fig. 16: in the left column, the proxies are shown for light pollution (top), and the OMI climatology for winter (middle) and summer (bottom). In columns 2 and 3, the synthetic satellite maps are shown if sampled by $26 \times 13\,km^2$ and $60 \times 30\,km^2$, respectively.

Now a "smoothing factor" can simply be defined as the ratio of the proxy and the simulated satellite mean at the measurement site, indicated by the white cross in Fig. 16. The resulting factors are summarized in Table 6. For winter, the smoothing effect has a smaller impact than in the other seasons, as the NO_2 gradients are low due to the longer NO_x lifetime. But in summer, the insufficient spatial resolution of the satellite instruments, especially of SCIAMACHY, can alone cause a deviation between MAX-DOAS and SCIAMACHY of about 46 % and between MAX-DOAS and OMI of about 14 % to 21 % (calculated from the OMI proxy). Based on the light proxy, the upper limits for the smoothing effect are 75 % for SCIAMACHY and 11–26 % for OMI.

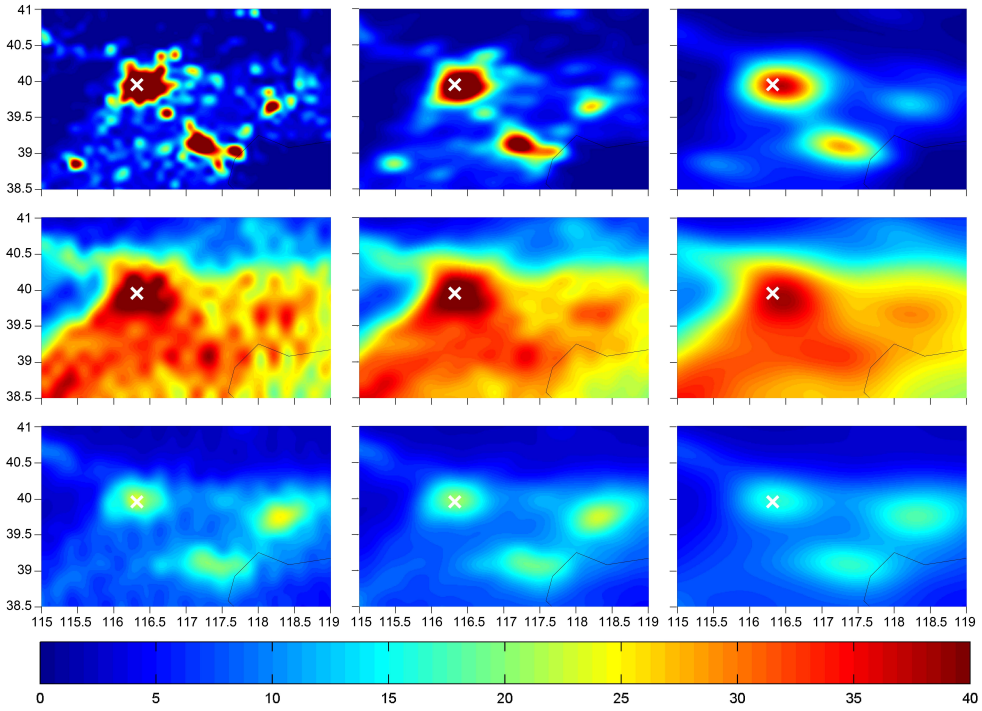

Fig. 16. Illustration of the "smoothing effect". Proxies for the "true" spatial distribution of NO_2 (left) are re-sampled by satellite pixels of $26 \times 13\,km^2$ (center) and $60 \times 30\,km^2$ (right). Proxies are nighttime lights (top) in artificial units, and seasonal mean NO_2 distributions from OMI for winter (middle) and summer (bottom) in units of 10^{15} molecules cm^{-2}. The white cross indicates the MAX-DOAS measurement site.

3.6.2 Aerosol shielding effect

In addition to the smoothing effect, the differences in the derived tropospheric NO_2 VCDs might partly also be attributed to the effects of aerosols on the satellite retrievals. The sensitivity of the satellite measurements can either be increased or decreased, depending on the aerosol optical properties and its vertical distribution relative to that of the trace gas of interest (Boersma et al., 2004; Martin et al., 2003; Leitão et al., 2010). If, for example, scattering aerosols are located within the NO_2 layer, the sensitivity of the satellite observations can be increased compared to aerosol-free observations. In contrast, a layer of aerosols above the NO_2 layer usually reduces the sensitivity of the satellite measurement (Leitão et al., 2010).

To investigate the effect of an assumed elevated aerosol layer, we calculated respective AMFs (or $DAMF_{\alpha,trop}$) with a radiative model, McArtim (Deutschmann, 2009; Deutschmann et al., 2011), and compared them with the AMFs (or $DAMF_{\alpha,trop}$) used in the satellite and MAX-DOAS retrievals. For the satellite observations we simulated AMFs for a detector located at 800 km altitude looking downwards in nadir direction; for the MAX-DOAS observations we simulated $DAMF_{30°,trop}$ (Eq. 8) for a viewing elevation angle of 30°.

In Beijing and its surrounding area, most of NO_x often accumulates in a surface layer near the traffic sources, while typical vertical distribution patterns of primary pollutants tend to result in the formation of secondary aerosols in the upper boundary layer (Ma et al., 2012). To reflect such conditions, we assumed a NO_2 profile extending from the surface to an altitude of 200m, while an aerosol profile of 0–1 km was used for all the simulations. These settings are referred to as the "elevated aerosol layer" in the following. Combinations of several aerosol optical depth (AOD) values, including 0, 0.1, 0.3, 0.5, 1.0, 2.0 and 3.0, and two single scattering albedo (SSA) values, i.e. 0.85 and 0.95, were selected for the simulations, based on previous measurements in Beijing (He et al., 2009; Garland et al., 2009; Wang et al., 2009). The simulations were performed at 420 nm wavelength, for selected solar zenith angles of 20°, 40°, 60°, and 80°, respectively, with a solar azimuth angle fixed at 180° and a surface albedo of 0.05.

The resulting values for the AMF and $DAMF_{30°,trop}$ were then compared to the respective values used in the satellite and MAX-DOAS retrievals. For MAX-DOAS observations, the ratio of the simulated $DAMF_{30°,trop}$ for elevated aerosol layers and the geometric approximation ((1–sin(30°))/sin(30°)) were calculated. For the satellite observations, the ratio of the simulated AMFs for elevated aerosol layers and the AMFs used in the SCIAMACHY standard

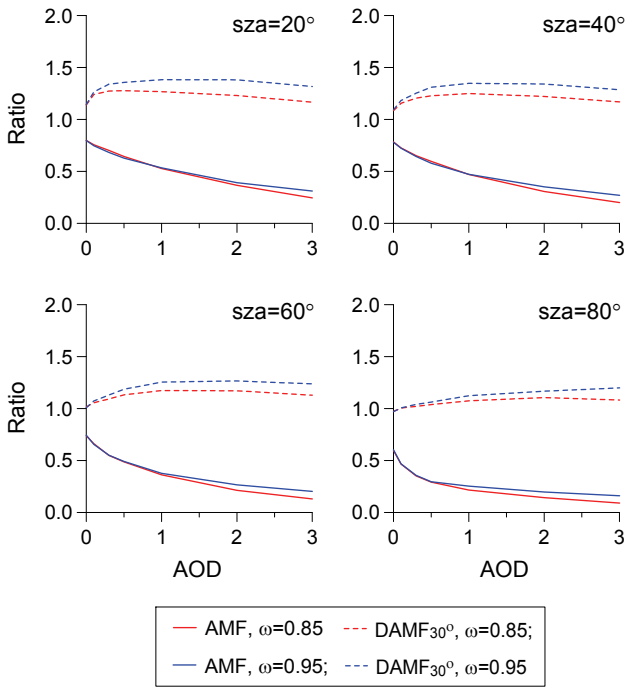

Fig. 17. Changes in the ratio of the simulated AMFs for elevated aerosol layers (an NO_2 profile of 0–200 m and an aerosol profile of 0–1 km) to the AMFs used in the standard satellite retrieval (the std95 profile for the SCIAMACHY retrieval) (solid lines), as well as the ratio of the simulated $DAMF_{30°,trop}$ for elevated aerosol layers to the geometric approximation used in the ground-based MAX-DOAS retrieval (dashed lines), as functions of aerosol optical depth (AOD) for single scattering albedos (ω) of 0.85 (red lines) and 0.95 (blue lines) and for different solar zenith angles (SZA), respectively.

retrieval (without considering aerosol effects) were calculated (here we used the standard AMF calculated for a profile with 95 % of the tropospheric NO_2 VCD below 1km as described in Sect. 3.6 for the SCIAMACHY retrieval). These ratios, if larger (or smaller) than unity, directly indicate the over- (or under-) estimation of the true tropospheric NO_2 VCD by the satellite and MAX-DOAS retrievals for the assumed case of an elevated aerosol layer (NO_2 layer from 0–200 m, aerosol layer from 0–1 km). The calculated ratios are shown in Fig. 17.

It is found that the satellite observations systematically underestimate the true tropospheric NO_2 VCD in cases of elevated aerosol layers. This underestimation increases with increasing aerosol optical depth and increasing solar zenith angle. In contrast, our MAX-DOAS observations tend to overestimate the true NO_2 VCDs in cases of elevated aerosol layers. However, this overestimation is much less pronounced than the underestimation of the satellite observations. Here it should be noted that the satellite results might not be fully representative for OMI observations, because in these retrievals different trace gas and aerosol profiles than for the SCIAMACHY MPI retrieval are used. In addition, part of the aerosol shielding effect will be even corrected by the cloud correction algorithm (aerosols are partly detected as clouds). Nevertheless, the general tendency that elevated aerosol layers cause an underestimation of the true tropospheric NO_2 VCD is the same, because (a) aerosols are typically less bright compared to clouds (single scattering albedo < 1) and (b) the vertical extent of the NO_2 layer assumed in the OMI retrieval is probably too high.

Table 7. Shielding factors, i.e. the ratio of "true" and approximately estimated tropospheric NO_2 VCD, for satellite and ground-based MAX-DOAS observations, calculated for the same environmental conditions as shown in Fig. 17, at AOD = 1.

SZA	Satellite		MAX-DOAS	
	$\omega = 0.85$	$\omega = 0.95$	$\omega = 0.85$	$\omega = 0.95$
20°	1.89	1.87	0.79	0.72
40°	2.13	2.12	0.80	0.74
60°	2.75	2.65	0.85	0.80
80°	4.63	3.94	0.93	0.89

Also, a "shielding factor" can be defined as the ratio of the "true" (with considering elevated aerosol layers in the AMF calculations) and approximately estimated (without considering aerosol effects) tropospheric NO_2 VCD. Such a shielding factor can simply be estimated using the reciprocal of the AMF and $DAMF_{30°,trop}$ ratios as shown in Fig. 17. Table 7 presents a summary of the shielding factors at a selected AOD value of unity. The shielding factors for ground-based MAX-DOAS measurements are slightly smaller than unity, indicating a little bit of overestimation of the true NO_2 VCDs in cases of elevated aerosol layers, as discussed above. However, the shielding factors for satellite observations are much larger, with a significant trend of increasing with SZA. For the overpass time of satellites (around 10:45 BJT for SCIAMACHY), the SZA reaches to its lowest value (about 25° for Beijing) in summer and the highest (about 67° for Beijing) in winter. These analyses indicate that elevated aerosol layers can cause a remarkable underestimation of the tropospheric NO_2 VCDs by satellite observations with respect to ground-based MAX-DOAS measurements, which can explain at least part of the observed differences between both datasets.

4 Summary and conclusions

We have retrieved tropospheric NO_2 vertical column densities (VCDs) over Beijing based on the three years' ground-based MAX-DOAS measurements from August 2008 to September 2011. Annual cycle and seasonally averaged diurnal variation patterns of the tropospheric NO_2 VCD over Beijing are obtained. The data also show a clear weekday/weekend effect and a post-Olympic effect of the tropospheric NO_2 VCD due to varying source emissions over

Beijing. We have also compared the tropospheric NO_2 VCDs derived from our ground MAX-DOAS measurements and from SCIAMACHY and OMI satellite data. While good correlation between satellite and MAX-DOAS observations is found, the results also show large systematic biases with the satellite retrievals being systematically lower with respect to the MAX-DOAS measurements.

Over the experiment period, the daytime mean tropospheric NO_2 VCDs (averaged between 08:00 and 17:00 BJT) over Beijing varied from 0.5 to 13.3 with an average of 3.6 during summertime, and from 0.2 to 16.8 with an average of 5.8 during wintertime (in units of 10^{16} molecules cm^{-2}). The annual cycles of the mean, median and maximum tropospheric NO_2 VCDs show clear maxima occurring in winter and minima in summer. The diurnal variation patterns of tropospheric NO_2 are rather different from one season to another, owing most probably to the variations of the emission strength and atmospheric lifetime. The VCD maximum occurred in the late morning during summer (4.8×10^{16} molecules cm^{-2} at 11:00 BJT), and in the late afternoon during winter (7.0×10^{16} molecules cm^{-2} at 17:00 BJT). The largest difference between the tropospheric NO_2 VCDs in different seasons took place in the afternoon.

In contrast to previous studies, we found a small weekly cycle of the tropospheric NO_2 VCD over Beijing. Here it is interesting to consider in detail the diurnal variation: The NO_2 VCD in the late afternoon was the largest (5.3×10^{16} molecules cm^{-2}) on Saturday and the lowest on Sunday (4.3×10^{16} molecules cm^{-2}). Such a "weekend effect" can be attributed to varying traffic situations in Beijing resulting from the different social and family activities during a week. We also found a clear maximum on Wednesday, which we cannot explain at the moment. Our data have shown clearly that the August tropospheric NO_2 VCDs were much smaller in 2008 than in the following years of 2009, 2010 and 2011, especially in the morning and early afternoon. The decrease in the tropospheric NO_2 VCD over Beijing during the 2008 Olympic Games is estimated to be 39–54 %, compared to the other years.

In contrast to satellite observations, ground-based MAX-DOAS instruments can measure the tropospheric NO_2 VCDs under both clear and cloudy conditions with almost similar sensitivity. Our measurements show that during 09:00–18:00 BJT, the differences in the tropospheric NO_2 VCD between the clear and cloudy conditions are typically 0.5–0.8×10^{16} molecules cm^{-2}, with an increase of 12–14 % from the clear to cloudy condition, most probably due to the lower photolysis rates of NO_2 below the clouds. Our data also show the effect of clouds on the color ratio, defined as ratio of the intensity at 320 nm (C320) to that at 434 nm (C434). This indicates that it is possible to use the C320/C434 ratio, measured by MAX-DOAS itself, as a threshold parameter to separate clear and cloudy conditions.

The tropospheric NO_2 VCDs derived by our ground MAX-DOAS measurements show a good correlation with SCIAMACHY and OMI satellite data, with a slightly higher correlation coefficient for SCIAMACHY ($R = 0.94$) than for OMI ($R = 0.91$–0.93). However, compared with the MAX-DOAS measurements, the satellite observations underestimate the tropospheric NO_2 VCDs over Beijing systematically, by 43 % for SCIAMACHY (2008–2010) and 26–38 % for OMI (2008–2011 DOMINO v2.0 and 2008–2009 DOMINO v1.02). The monthly mean tropospheric NO_2 VCDs measured by MAX-DOAS are typically 1.2–2.9 times as large as those retrieved by SCIAMACHY, and 1.1–1.5 times as large as those retrieved by DOMINO v2.0.

This systematic underestimation might be caused by two main effects. First, the satellite observations do not fully resolve the horizontal gradients close to strong emission sources, but also average over neighboring areas containing systematically smaller values. Second, the different profile heights of NO_2 and aerosols probably lead to a systematic underestimation of the true tropospheric NO_2 VCDs in the satellite retrievals, while the MAX-DOAS observations are almost not affected. Since the atmospheric lifetime of NO_2 is systematically shorter than that of aerosols, the aerosols will typically be well mixed throughout the boundary layer, while the NO_2 concentrations rapidly decrease with altitude. We simulated the effect of such conditions on the satellite and MAX-DOAS measurements assuming that the NO_2 is confined within the lowest 200 m while the aerosols are located between the surface and 1000 m. In contrast to the smoothing effect, which is weaker in winter than in summer, the aerosol shielding effect becomes stronger with increasing solar zenith angle and thus should be more efficient in winter than in summer, given the same aerosol optical and profile conditions. While the smoothing factors, i.e. the ratio of "true" and smoothed NO_2 VCD at the measurement site, are estimated to be 1–2 for satellite observations over Beijing, the shielding factors, defined as the "true" and approximately estimated (without considering aerosol effects) NO_2 VCD, are 2–3 for typical aerosol conditions in Beijing. Such an aerosol shielding effect can be large enough to explain the underestimation of the tropospheric NO_2 VCDs over Beijing by SCIAMACHY and OMI with respect to the ground-based MAX-DOAS measurements, while the gradient smoothing effect could play an additional role.

Acknowledgements. This work was supported by the NSFC (grant No. 41075095) and the CMA (grant Nos. GYHY200706005 and GYHY201206015). We are grateful to Jos Lelieveld of MPIC and Cunde Xiao of CAMS for their help to initiate this research and Hao Peng and Junrang Guo of CAMS for technically assisting to set up and maintain the measurements. We acknowledge the free use of tropospheric NO_2 column data from the OMI sensor (http://www.temis.nl) and nighttime light data measured by DMSP (US Air Force Weather Agency) and processed by NOAA's National Geophysical Data Center

(http://www.ngdc.noaa.gov/dmsp/). We also thank the guest editor Xuexi Tie for handling this manuscript and the two anonymous reviewers for their constructive comments on the manuscript.

Edited by: X. Tie

References

Beirle, S. and Wagner, T.: Tropospheric vertical column densities of NO_2 from SCIAMACHY, available at: http://www.sciamachy.org/products/NO2/NO2vc_v0_9_MPI_AD.pdf (last access: October 2012), 2010.

Beirle, S., Platt, U., Wenig, M., and Wagner, T.: Weekly cycle of NO_2 by GOME measurements: a signature of anthropogenic sources, Atmos. Chem. Phys., 3, 2225–2232, doi:10.5194/acp-3-2225-2003, 2003.

Beirle, S., Kühl, S., Pukite, J., and Wagner, T.: Retrieval of tropospheric column densities of NO_2 from combined SCIAMACHY nadir/limb measurements, Atmos. Meas. Tech., 3, 283–299, doi:10.5194/amt-3-283-2010, 2010.

Boersma, K. F., Eskes, H. J., and Brinksma, E. J.: Error analysis for tropospheric NO_2 retrieval from space, J. Geophys. Res., 109, D04311, doi:10.1029/2003jd003962, 2004.

Boersma, K. F., Eskes, H. J., Veefkind, J. P., Brinksma, E. J., van der A, R. J., Sneep, M., van den Oord, G. H. J., Levelt, P. F., Stammes, P., Gleason, J. F., and Bucsela, E. J.: Near-real time retrieval of tropospheric NO_2 from OMI, Atmos. Chem. Phys., 7, 2103–2118, doi:10.5194/acp-7-2103-2007, 2007.

Boersma, K. F., Eskes, H. J., Dirksen, R. J., van der A, R. J., Veefkind, J. P., Stammes, P., Huijnen, V., Kleipool, Q. L., Sneep, M., Claas, J., Leitão, J., Richter, A., Zhou, Y., and Brunner, D.: An improved tropospheric NO_2 column retrieval algorithm for the Ozone Monitoring Instrument, Atmos. Meas. Tech., 4, 1905–1928, doi:10.5194/amt-4-1905-2011, 2011.

Bovensmann, H., Burrows, J. P., Buchwitz, M., Frerick, J., Noël, S., Rozanov, V. V., Chance, K. V., and Goede, A. P. H.: SCIAMACHY: Mission objectives and measurement modes, J. Atmos. Sci., 56, 127–150, 1999.

Brinksma, E. J., Pinardi, G., Volten, H., Braak, R., Richter, A., Schönhardt, A., van Roozendael, M., Fayt, C., Hermans, C., Dirksen, R. J., Vlemmix, T., Berkhout, A. J. C., Swart, D. P. J., Oetjen, H., Wittrock, F., Wagner, T., Ibrahim, O. W., de Leeuw, G., Moerman, M., Curier, R. L., Celarier, E. A., Cede, A., Knap, W. H., Veefkind, J. P., Eskes, H. J., Allaart, M., Rothe, R., Piters, A. J. M., and Levelt, P. F.: The 2005 and 2006 DANDELIONS NO_2 and aerosol intercomparison campaigns, J. Geophys. Res., 113, D16S46, doi:10.1029/2007jd008808, 2008.

Burrows, J. P., Richter, A., Dehn, A., Deters, B., Himmelmann, S., Voigt, S., and Orphal, J.: Atmospheric remote sensing reference data from GOME-2. temperature-dependent absorption cross-sections of O_3 in the 231–794 nm range, J. Quant. Spectrosc. Ra., 61, 509–517, 1999a.

Burrows, J. P., Weber, M., Buchwitz, M., Rozanov, V. V., Ladstätter-Weißenmayer, A., Richter, A., DeBeek, R., Hoogen, R., Brmstedt, K., and Eichmann, K. U.: The global ozone monitoring experiment (GOME): mission concept and first scientific results, J. Atmos. Sci., 56, 151–175, 1999b.

Celarier, E. A., Brinksma, E. J., Gleason, J. F., Veefkind, J. P., Cede, A., Herman, J. R., Ionov, D., Goutail, F., Pommereau, J. P., Lambert, J. C., van Roozendael, M., Pinardi, G., Wittrock, F., Schönhardt, A., Richter, A., Ibrahim, O. W., Wagner, T., Bojkov, B., Mount, G., Spinei, E., Chen, C. M., Pongetti, T. J., Sander, S. P., Bucsela, E. J., Wenig, M. O., Swart, D. P. J., Volten, H., Kroon, M., and Levelt, P. F.: Validation of Ozone Monitoring Instrument nitrogen dioxide columns, J. Geophys. Res., 113, D15S15, doi:10.1029/2007jd008908, 2008.

Chen, D., Zhou, B., Beirle, S., Chen, L. M., and Wagner, T.: Tropospheric NO_2 column densities deduced from zenith-sky DOAS measurements in Shanghai, China, and their application to satellite validation, Atmos. Chem. Phys., 9, 3641–3662, doi:10.5194/acp-9-3641-2009, 2009.

Chou, C. C.-K., Tsai, C.-Y., Chang, C.-C., Lin, P.-H., Liu, S. C., and Zhu, T.: Photochemical production of ozone in Beijing during the 2008 Olympic Games, Atmos. Chem. Phys., 11, 9825–9837, doi:10.5194/acp-11-9825-2011, 2011.

Cinzano, P., Falchi, F., and Elvidge, C. D.: The first world atlas of the artificial night sky brightness, Mon. Not. R. Astron. Soc., 328, 689–707, 2001.

Clémer, K., Van Roozendael, M., Fayt, C., Hendrick, F., Hermans, C., Pinardi, G., Spurr, R., Wang, P., and De Mazière, M.: Multiple wavelength retrieval of tropospheric aerosol optical properties from MAXDOAS measurements in Beijing, Atmos. Meas. Tech., 3, 863–878, doi:10.5194/amt-3-863-2010, 2010.

Deutschmann, T.: Atmospheric radiative transfer modelling using Monte Carlo methods, Diploma Thesis, University of Heidelberg, Heidelberg, Germany, 2009.

Deutschmann, T., Beirle, S., Frieß, U., Grzegorski, M., Kern, C., Kritten, L., Platt, U., Prados-Román, C., Puite, J., Wagner, T., Werner, B., and Pfeilsticker, K.: The Monte Carlo atmospheric radiative transfer model McArtim: Introduction and validation of Jacobians and 3D features, J. Quant. Spectrosc. Ra., 112, 1119–1137, 2011.

EPA: Air Quality Index-A Guide to Air Quality and Your Health, United States Environmental Protection Agency, Washington, DC20460, EPA-454/R-00-005, 2000.

Fayt, C. and Van Roozendael, M.: WinDOAS 2.1 software user manual, IASB/BIRA Uccle, Belgium, 2001.

Garland, R. M., Schmid, O., Nowak, A., Achtert, P., Wiedensohler, A., Gunthe, S. S., Takegawa, N., Kita, K., Kondo, Y., Hu, M., Shao, M., Zeng, L. M., Zhu, T., Andreae, M. O., and Pöschl, U.: Aerosol optical properties observed during Campaign of Air Quality Research in Beijing 2006 (CAREBeijing-2006): Characteristic differences between the inflow and outflow of Beijing city air, J. Geophys. Res., 114, D00G04, doi:10.1029/2008jd010780, 2009.

Greenblatt, G. D., Orlando, J. J., Burkholder, J. B., and Ravishankara, A. R.: Absorption measurements of oxygen between 330 and 1140 nm, J. Geophys. Res., 95, 18577–18582, doi:10.1029/JD095iD11p18577, 1990.

Hönninger, G., von Friedeburg, C., and Platt, U.: Multi axis differential optical absorption spectroscopy (MAX-DOAS), Atmos. Chem. Phys., 4, 231–254, doi:10.5194/acp-4-231-2004, 2004.

Hains, J. C., Boersma, K. F., Kroon, M., Dirksen, R. J., Cohen, R. C., Perring, A. E., Bucsela, E., Volten, H., Swart, D. P. J., Richter, A., Wittrock, F., Schoenhardt, A., Wagner, T., Ibrahim, O. W., van Roozendael, M., Pinardi, G., Gleason, J. F., Veefkind, J. P., and Levelt, P.: Testing and improving OMI DOMINO tropospheric NO_2 using observations from the DANDELIONS and

INTEX-B validation campaigns, J. Geophys. Res., 115, D05301, doi:10.1029/2009jd012399, 2010.

Hayn, M., Beirle, S., Hamprecht, F. A., Platt, U., Menze, B. H., and Wagner, T.: Analysing spatio-temporal patterns of the global NO_2-distribution retrieved from GOME satellite observations using a generalized additive model, Atmos. Chem. Phys., 9, 6459–6477, doi:10.5194/acp-9-6459-2009, 2009.

He, X., Li, C. C., Lau, A. K. H., Deng, Z. Z., Mao, J. T., Wang, M. H., and Liu, X. Y.: An intensive study of aerosol optical properties in Beijing urban area, Atmos. Chem. Phys., 9, 8903–8915, doi:10.5194/acp-9-8903-2009, 2009.

Ibrahim, O., Shaiganfar, R., Sinreich, R., Stein, T., Platt, U., and Wagner, T.: Car MAX-DOAS measurements around entire cities: quantification of NO_x emissions from the cities of Mannheim and Ludwigshafen (Germany), Atmos. Meas. Tech., 3, 709–721, doi:10.5194/amt-3-709-2010, 2010.

Irie, H., Kanaya, Y., Akimoto, H., Tanimoto, H., Wang, Z., Gleason, J. F., and Bucsela, E. J.: Validation of OMI tropospheric NO_2 column data using MAX-DOAS measurements deep inside the North China Plain in June 2006: Mount Tai Experiment 2006, Atmos. Chem. Phys., 8, 6577–6586, doi:10.5194/acp-8-6577-2008, 2008.

Jiang, W. H., Ma, J. Z., Yan, P., Richter, A., Burrows, J. P., and Nüß, H.: Characterization of NO_2 pollution changes in Beijing using GOME satellite data, J. Appl. Meteor. Sci, 17, 67–72, 2006.

Jin, X., Xie, P. H., Si, F. Q., Dou, K., Li, A., Liu, Y., and Liu, W. Q.: Retrieval of tropospheric NO_2 by Multi Axis Differential Optical Absorption Spectroscopy, Spectrosc. Spect. Anal., 30, 2464–2469, 2010.

Kramer, L. J., Leigh, R. J., Remedios, J. J., and Monks, P. S.: Comparison of OMI and ground-based in situ and MAX-DOAS measurements of tropospheric nitrogen dioxide in an urban area, J. Geophys. Res., 113, D16S39, doi:10.1029/2007jd009168, 2008.

Kraus, S.: DOASIS, DOAS for Windows software [CD-ROM], in: Proceedings of the 1st International DOAS-Workshop, Heidelberg, Germany, 13–14 September 2001, 2001.

Leitão, J., Richter, A., Vrekoussis, M., Kokhanovsky, A., Zhang, Q. J., Beekmann, M., and Burrows, J. P.: On the improvement of NO_2 satellite retrievals – aerosol impact on the airmass factors, Atmos. Meas. Tech., 3, 475–493, doi:10.5194/amt-3-475-2010, 2010.

Lelieveld, J. and Dentener, F. J.: What controls tropospheric ozone?, J. Geophys. Res., 105, 3531–3551, doi:10.1029/1999jd901011, 2000.

Lelieveld, J., Peters, W., Dentener, F. J., and Krol, M. C.: Stability of tropospheric hydroxyl chemistry, J. Geophys. Res., 107, 4715, doi:10.1029/2002jd002272, 2002.

Levelt, P., Van den Oord, G., Dobber, M., Malkki, A., Visser, H., de Vries, J., Stammes, P., Lundell, J., and Saari, H.: The Ozone Monitoring Instrument, IEEE T. Geosci. Remote, 44, 1093–1101, doi:10.1109/TGRS.2006.872333, 2006.

Li, X., Brauers, T., Hofzumahaus, A., Lu, K., Li, Y. P., Shao, M., Wagner, T., and Wahner, A.: MAX-DOAS measurements of NO_2, HCHO and CHOCHO at a rural site in Southern China, Atmos. Chem. Phys. Discuss., 12, 3983–4029, doi:10.5194/acpd-12-3983-2012, 2012.

Lin, J.-T.: Satellite constraint for emissions of nitrogen oxides from anthropogenic, lightning and soil sources over East China on a high-resolution grid, Atmos. Chem. Phys., 12, 2881–2898, doi:10.5194/acp-12-2881-2012, 2012.

Lin, J.-T. and McElroy, M. B.: Detection from space of a reduction in anthropogenic emissions of nitrogen oxides during the Chinese economic downturn, Atmos. Chem. Phys., 11, 8171–8188, doi:10.5194/acp-11-8171-2011, 2011.

Lin, J.-T., McElroy, M. B., and Boersma, K. F.: Constraint of anthropogenic NO_x emissions in China from different sectors: a new methodology using multiple satellite retrievals, Atmos. Chem. Phys., 10, 63–78, doi:10.5194/acp-10-63-2010, 2010.

Lin, W., Xu, X., Ge, B., and Liu, X.: Gaseous pollutants in Beijing urban area during the heating period 2007–2008: variability, sources, meteorological, and chemical impacts, Atmos. Chem. Phys., 11, 8157–8170, doi:10.5194/acp-11-8157-2011, 2011.

Lu, K., Zhang, Y., Su, H., Brauers, T., Chou, C. C., Hofzumahaus, A., Liu, S. C., Kita, K., Kondo, Y., Shao, M., Wahner, A., Wang, J., Wang, X., and Zhu, T.: Oxidant (O_3 + NO_2) production processes and formation regimes in Beijing, J. Geophys. Res., 115, D07303, doi:10.1029/2009jd012714, 2010.

Ma, J., Richter, A., Burrows, J. P., Nüß, H., and van Aardenne, J. A.: Comparison of model-simulated tropospheric NO_2 over China with GOME-satellite data, Atmos. Environ., 40, 593–604, 2006.

Ma, J. Z., Wang, W., Chen, Y., Liu, H. J., Yan, P., Ding, G. A., Wang, M. L., Sun, J., and Lelieveld, J.: The IPAC-NC field campaign: a pollution and oxidization pool in the lower atmosphere over Huabei, China, Atmos. Chem. Phys., 12, 3883–3908, doi:10.5194/acp-12-3883-2012, 2012.

Martin, R. V., Jacob, D. J., Chance, K., Kurosu, T. P., Palmer, P. I., and Evans, M. J.: Global inventory of nitrogen oxide emissions constrained by space-based observations of NO_2 columns, J. Geophys. Res., 108, 4537, doi:10.1029/2003jd003453, 2003.

Mijling, B., van der A, R. J., Boersma, K. F., Van Roozendael, M., De Smedt, I., and Kelder, H. M.: Reductions of NO_2 detected from space during the 2008 Beijing Olympic Games, Geophys. Res. Lett., 36, L13801, doi:10.1029/2009gl038943, 2009.

Molina, M. J. and Molina, L. T.: Megacities and atmospheric pollution, J. Air Waste Manage. Assoc. , 54, 644–680, 2004.

Parrish, D. D. and Zhu, T.: Clean Air for Megacities, Science, 326, 674–675, doi:10.1126/science.1176064, 2009.

Piters, A. J. M., Boersma, K. F., Kroon, M., Hains, J. C., Van Roozendael, M., Wittrock, F., Abuhassan, N., Adams, C., Akrami, M., Allaart, M. A. F., Apituley, A., Beirle, S., Bergwerff, J. B., Berkhout, A. J. C., Brunner, D., Cede, A., Chong, J., Clémer, K., Fayt, C., Frieß, U., Gast, L. F. L., Gil-Ojeda, M., Goutail, F., Graves, R., Griesfeller, A., Großmann, K., Hemerijckx, G., Hendrick, F., Henzing, B., Herman, J., Hermans, C., Hoexum, M., van der Hoff, G. R., Irie, H., Johnston, P. V., Kanaya, Y., Kim, Y. J., Klein Baltink, H., Kreher, K., de Leeuw, G., Leigh, R., Merlaud, A., Moerman, M. M., Monks, P. S., Mount, G. H., Navarro-Comas, M., Oetjen, H., Pazmino, A., Perez-Camacho, M., Peters, E., du Piesanie, A., Pinardi, G., Puentedura, O., Richter, A., Roscoe, H. K., Schönhardt, A., Schwarzenbach, B., Shaiganfar, R., Sluis, W., Spinei, E., Stolk, A. P., Strong, K., Swart, D. P. J., Takashima, H., Vlemmix, T., Vrekoussis, M., Wagner, T., Whyte, C., Wilson, K. M., Yela, M., Yilmaz, S., Zieger, P., and Zhou, Y.: The Cabauw Intercomparison campaign for Nitrogen Dioxide measuring Instruments (CINDI): design, execution, and early results, Atmos. Meas. Tech., 5, 457–485, doi:10.5194/amt-5-457-2012, 2012.

Platt, U.: Differential optical absorption spectroscopy (DOAS), in: Air Monitoring by Spectroscopic Techniques, edited by: Sigrist, M. W., Chemical Analysis Series, 127, John Wiley, New York, 27–84, 1994.

Platt, U. and Stutz, J.: Differential Optical Absorption Spectroscopy Principles and Applications, Series: Physics of Earth and Space Environments, Springer, Heidelberg, 597 pp., 2008.

Richter, A., Burrows, J. P., Nusz, H., Granier, C., and Niemeier, U.: Increase in tropospheric nitrogen dioxide over China observed from space, Nature, 437, 129–132, doi:10.1038/nature04092, 2005.

Richter, A., Wittrock, F., Heckel, A., and Burrows, J. P.: Monitoring Changes in Tropospheric Constitution from Space, annual report to ACCENT-TROPOSAT-2 (AT2), Task Group 1, available at: http://www.doas-bremen.de/reports/accent_richter_report_4thyear.pdf (last access: October 2012), 2008.

Richter, A., Begoin, M., Hilboll, A., and Burrows, J. P.: An improved NO_2 retrieval for the GOME-2 satellite instrument, Atmos. Meas. Tech., 4, 1147–1159, doi:10.5194/amt-4-1147-2011, 2011.

Sarkissian, A., Pommereau, J., Pierre, Goutail, F., and Kyro, E.: PSC and volcanic aerosol observations during EASOE by UV-visible ground-based spectrometry, Geophys. Res. Lett., 21, 1319–1322, doi:10.1029/93gl03072, 1994.

Seinfeld, J. H. and Pandis, S. N.: Atmospheric Chemistry and Physics, John Wiley and Sons., New York, 1998.

SEPA: Ambient air quality standard, People's Repulic of China National Standard GB 3095-1996, 1996.

Shaiganfar, R., Beirle, S., Sharma, M., Chauhan, A., Singh, R. P., and Wagner, T.: Estimation of NO_x emissions from Delhi using Car MAX-DOAS observations and comparison with OMI satellite data, Atmos. Chem. Phys., 11, 10871–10887, doi:10.5194/acp-11-10871-2011, 2011.

Shi, C. N., Fernando, H. J. S., Wang, Z. F., An, X. Q., and Wu, Q. Z.: Tropospheric NO_2 columns over East Central China: Comparisons between SCIAMACHY measurements and nested CMAQ simulations, Atmos. Environ., 42, 7165–7173, doi:10.1016/j.atmosenv.2008.05.046, 2008.

Solomon, S., Portmann, R. W., Sanders, R. W., Daniel, J. S., Madsen, W., Bartram, B., and Dutton, E. G.: On the role of nitrogen dioxide in the absorption of solar radiation, J. Geophys. Res., 104, 12047–12058, doi:10.1029/1999jd900035, 1999.

Stone, R.: Beijing's Marathon Run to Clean Foul Air Nears Finish Line, Science, 321, 636–637, doi:10.1126/science.321.5889.636, 2008.

Sun, J., Zhang, Q., Canagaratna, M. R., Zhang, Y., Ng, N. L., Sun, Y., Jayne, J. T., Zhang, X., Zhang, X., and Worsnop, D. R.: Highly time- and size-resolved characterization of submicron aerosol particles in Beijing using an Aerodyne Aerosol Mass Spectrometer, Atmos. Environ., 44, 131–140, 2010.

Tang, G., Li, X., Wang, Y., Xin, J., and Ren, X.: Surface ozone trend details and interpretations in Beijing, 2001–2006, Atmos. Chem. Phys., 9, 8813–8823, doi:10.5194/acp-9-8813-2009, 2009.

Valks, P., Pinardi, G., Richter, A., Lambert, J.-C., Hao, N., Loyola, D., Van Roozendael, M., and Emmadi, S.: Operational total and tropospheric NO_2 column retrieval for GOME-2, Atmos. Meas. Tech., 4, 1491–1514, doi:10.5194/amt-4-1491-2011, 2011.

van der A, R. J., Peters, D. H. M. U., Eskes, H., Boersma, K. F., Van Roozendael, M., De Smedt, I., and Kelder, H. M.: Detection of the trend and seasonal variation in tropospheric NO_2 over China, J. Geophys. Res., 111, D12317, doi:10.1029/2005jd006594, 2006.

van der A, R. J., Eskes, H. J., Boersma, K. F., van Noije, T. P. C., Van Roozendael, M., De Smedt, I., Peters, D. H. M. U., and Meijer, E. W.: Trends, seasonal variability and dominant NO_x source derived from a ten year record of NO2 measured from space, J. Geophys. Res., 113, D04302, doi:10.1029/2007jd009021, 2008.

Vandaele, A. C., Hermans, C., Simon, P. C., Carleer, M., Colin, R., Fally, S., Mérienne, M. F., Jenouvrier, A., and Coquart, B.: Measurements of the NO_2 absorption cross-section from 42 000 cm^{-1} to 10 000 cm^{-1} (238–1000 nm) at 220 K and 294 K, J. Quant. Spectrosc. Ra., 59, 171–184, 1998.

Wagner, T., Dix, B., Friedeburg, C. v., Frieß, U., Sanghavi, S., Sinreich, R., and Platt, U.: MAX-DOAS O_4 measurements: A new technique to derive information on atmospheric aerosols – Principles and information content, J. Geophys. Res., 109, D22205, doi:10.1029/2004jd004904, 2004.

Wagner, T., Beirle, S., Deutschmann, T., Eigemeier, E., Frankenberg, C., Grzegorski, M., Liu, C., Marbach, T., Platt, U., and Penning de Vries, M.: Monitoring of atmospheric trace gases, clouds, aerosols and surface properties from UV/vis/NIR satellite instruments, J. Opt. A: Pure Appl. Opt., 10, 104019, doi:10.1088/1464-4258/10/10/104019, 2008.

Wagner, T., Deutschmann, T., and Platt, U.: Determination of aerosol properties from MAX-DOAS observations of the Ring effect, Atmos. Meas. Tech., 2, 495–512, doi:10.5194/amt-2-495-2009, 2009.

Wagner, T., Ibrahim, O., Shaiganfar, R., and Platt, U.: Mobile MAX-DOAS observations of tropospheric trace gases, Atmos. Meas. Tech., 3, 129–140, doi:10.5194/amt-3-129-2010, 2010.

Wang, S. X., Zhao, M., Xing, J., Wu, Y., Zhou, Y., Lei, Y., He, K. B., Fu, L. X., and Hao, J. M.: Quantifying the air pollutants emission reduction during the 2008 Olympic Games in Beijing, Environ. Sci. Technol., 44, 2490–2496, doi:10.1021/es9028167, 2010a.

Wang, T., Nie, W., Gao, J., Xue, L. K., Gao, X. M., Wang, X. F., Qiu, J., Poon, C. N., Meinardi, S., Blake, D., Wang, S. L., Ding, A. J., Chai, F. H., Zhang, Q. Z., and Wang, W. X.: Air quality during the 2008 Beijing Olympics: secondary pollutants and regional impact, Atmos. Chem. Phys., 10, 7603–7615, doi:10.5194/acp-10-7603-2010, 2010b.

Wang, Y., McElroy, M. B., Boersma, K. F., Eskes, H. J., and Veefkind, J. P.: Traffic restrictions associated with the Sino-African summit: Reductions of NO_x detected from space, Geophys. Res. Lett., 34, L08814, doi:10.1029/2007gl029326, 2007a.

Wang, Y., McElroy, M. B., Martin, R. V., Streets, D. G., Zhang, Q., and Fu, T.-M.: Seasonal variability of NO_x emissions over east China constrained by satellite observations: Implications for combustion and microbial sources, J. Geophys. Res., 112, D06301, doi:10.1029/2006jd007538, 2007b.

Wang, Y., Che, H., Ma, J., Wang, Q., Shi, G., Chen, H., Goloub, P., and Hao, X.: Aerosol radiative forcing under clear, hazy, foggy, and dusty weather conditions over Beijing, China, Geophys. Res. Lett., 36, L06804, doi:10.1029/2009gl037181, 2009.

Witte, J. C., Schoeberl, M. R., Douglass, A. R., Gleason, J. F., Krotkov, N. A., Gille, J. C., Pickering, K. E., and Livesey, N.: Satellite observations of changes in air quality during the 2008 Beijing Olympics and Paralympics, Geophys. Res. Lett., 36, L17803, doi:10.1029/2009gl039236, 2009.

Wittrock, F., Oetjen, H., Richter, A., Fietkau, S., Medeke, T., Rozanov, A., and Burrows, J. P.: MAX-DOAS measurements of atmospheric trace gases in Ny-Ålesund – Radiative transfer studies and their application, Atmos. Chem. Phys., 4, 955–966, doi:10.5194/acp-4-955-2004, 2004.

Xu, J., Ma, J. Z., Zhang, X. L., Xu, X. B., Xu, X. F., Lin, W. L., Wang, Y., Meng, W., and Ma, Z. Q.: Measurements of ozone and its precursors in Beijing during summertime: impact of urban plumes on ozone pollution in downwind rural areas, Atmos. Chem. Phys., 11, 12241–12252, doi:10.5194/acp-11-12241-2011, 2011.

Yu, H., Wang, P. C., Zong, X. M., Li, X., and Lu, D. R.: Change of NO_2 column density over Beijing from satellite measurement during the Beijing 2008 Olympic Games, Chin. Sci. Bull., 55, 308–313, doi:10.1007/s11434-009-0375-0, 2010.

Zhang, X. Y., Zhang, P., Zhang, Y., Li, X. J., and Qiu, H.: The trend, seasonal cycle, and sources of tropospheric NO_2 over China during 1997-2006 based on satellite measurement, Sci. China Ser. D-Earth Sci., 50, 1877–1884, doi:10.1007/s11430-007-0141-6, 2007.

Zhao, B., Wang, P., Ma, J. Z., Zhu, S., Pozzer, A., and Li, W.: A high-resolution emission inventory of primary pollutants for the Huabei region, China, Atmos. Chem. Phys., 12, 481–501, doi:10.5194/acp-12-481-2012, 2012.

Zhao, C. S., Tie, X. X., Wang, G. L., Qin, Y., and Yang, P. C.: Analysis of air quality in eastern China and its interaction with other regions of the world, J. Atmos. Chem., 55, 189–204, doi:10.1007/s10874-006-9022-1, 2006.

Zhu, Y. W., Liu, W. Q., Hua, X. P., Dou, K., Si, F. Q., Li, S. W., Zhang, Y. H., and Qin, M.: Monitoring and analysis of atmospheric pollutants in traffic ban period of Beijing with DOAS, Ac. Photon. Sin., 38, 2040–2045, 2009.

Zhu, Y. W., Liu, W. Q., Fang, J., Xie, P. H., Dou, K., Qin, M., and Si, F. Q.: Monitoring and analysis of vertical profile of atmospheric HONO and NO_2 in the boundary layer of Beijing, Spectrosc. Spect. Anal., 31, 1078–1082, 2010.